Hydrol. Earth Syst. Sci., 16, 1745–1773, 2012
www.hydrol-earth-syst-sci.net/16/1745/2012/
doi:10.5194/hess-16-1745-2012

Hydrology and Earth System Sciences

Evaluation of the ISBA-TRIP continental hydrologic system over the Niger basin using in situ and satellite derived datasets

V. Pedinotti[1,2], A. Boone[1], B. Decharme[1], J. F. Crétaux[3], N. Mognard[3], G. Panthou[4], F. Papa[3], and B. A. Tanimoun[5]

[1]Groupe d'étude de l'atmosphère météorologique (GAME), URA1357, CNRS – Météo-France, Toulouse, France
[2]Centre National d'études spatiales (CNES), Toulouse, France
[3]Laboratoire d'Etudes en Géophysique et Océanographie Spatiales (LEGOS), Toulouse, France
[4]Laboratoire d'étude des Transferts en Hydrologie et Environnement (LTHE), Grenoble, France
[5]Autorité du Bassin du Niger (ABN), Niamey, Niger

Correspondence to: V. Pedinotti (vanessa.pedinotti@gmail.com)

Received: 30 September 2011 – Published in Hydrol. Earth Syst. Sci. Discuss.: 14 October 2011
Revised: 18 May 2012 – Accepted: 22 May 2012 – Published: 26 June 2012

Abstract. During the 1970s and 1980s, West Africa has faced extreme climate variations with extended drought conditions. Of particular importance is the Niger basin, since it traverses a large part of the Sahel and is thus a critical source of water for an ever-increasing local population in this semi arid region. However, the understanding of the hydrological processes over this basin is currently limited by the lack of spatially distributed surface water and discharge measurements. The purpose of this study is to evaluate the ability of the ISBA-TRIP continental hydrologic system to represent key processes related to the hydrological cycle of the Niger basin. ISBA-TRIP is currently used within a coupled global climate model, so that the scheme must represent the first order processes which are critical for representing the water cycle while retaining a limited number of parameters and a simple representation of the physics. To this end, the scheme uses first-order approximations to account explicitly for the surface river routing, the floodplain dynamics, and the water storage using a deep aquifer reservoir. In the current study, simulations are done at a 0.5 by 0.5° spatial resolution over the 2002–2007 period (in order to take advantage of the recent satellite record and data from the African Monsoon Multidisciplinary Analyses project, AMMA). Four configurations of the model are compared to evaluate the separate impacts of the flooding scheme and the aquifer on the water cycle. Moreover, the model is forced by two different rainfall datasets to consider the sensitivity of the model to rainfall input uncertainties. The model is evaluated using in situ discharge measurements as well as satellite derived flood extent, total continental water storage changes and river height changes. The basic analysis of in situ discharges confirms the impact of the inner delta area, known as a significant flooded area, on the discharge, characterized by a strong reduction of the streamflow after the delta compared to the streamflow before the delta. In the simulations, the flooding scheme leads to a non-negligible increase of evaporation over large flooded areas, which decreases the Niger river flow by 15 % to 50 % in the locations situated after the inner delta as a function of the input rainfall dataset used as forcing. This improves the simulation of the river discharge downstream of the delta, confirming the need for coupling the land surface scheme with the flood model. The deep aquifer reservoir improves Niger low flows and the recession law during the dry season. The comparison with 3 satellite products from the Gravity Recovery and Climated Experiment (GRACE) shows a non negligible contribution of the deeper soil layers to the total storage (34 % for groundwater and aquifer). The simulations also show a non negligible sensitivity of the simulations to rain uncertainties especially concerning the discharge. Finally, sensitivity tests show that a good parameterization of routing is required to optimize simulation errors. Indeed, the modification of certain key parameters which can be observed from space (notably river height and flooded zones height changes and extent) has an impact on the model dynamics, thus it is suggested that improving the model input parameters using future developments in remote sensing technologies such as the joint CNES-NASA satellite project SWOT (Surface Water Ocean Topography), which will provide water heights and extentat land surface with an unprecedented 50–100 m resolution and precision.

Published by Copernicus Publications on behalf of the European Geosciences Union.

1 Introduction

Over the past 5 decades, West Africa has faced extreme climate variations with extended extreme drought conditions most recently during the 70s and 80s (Ali and Lebel, 2009). In this region, precipitation is closely linked with the monsoon, and better understanding and prediction are needed for improved water resource management. With an approximate length of 4180 km (2600 miles), the Niger river is the largest river in West Africa. It starts in the Guinea Highlands in southeastern Guinea and ends in Nigeria, discharging through a massive delta into the Gulf of Guinea within the Atlantic Ocean. It is a significant source of water and food for West Africa which, as an agricultural region, is highly dependent on the water availability and management practices.

According to several studies (Coe, 1998; Andersen et al., 2005; Dadson et al., 2010), the seasonal and interannual cycle of the Niger river discharge is influenced by the hydrological processes, including overland processes (precipitation, evaporation, stream flows, floods, infiltration, etc.) and underground processes (groundwater and/or deep aquifer recharge). These processes are theorized to have feedbacks with the climate, rainfall variability and the carbon cycle (Houwelling et al., 1999; Matthews, 2000; Bousquet et al., 2006; Taylor, 2010; Taylor et al., 2011). Thus, a better parameterization of hydrological processes in atmospheric general circulation models (AGCMs) is necessary to obtain a better understanding of the feedbacks with the West African monsoon. This could then potentially translate into improved water resource management and climate prediction, at least at the regional scale (Gedney et al., 2000; Douville et al., 2000, 2003, 2004; Molod et al., 2004; Lawrence and Slater, 2007; Alkama et al., 2008).

Currently, the representation of the surface component of the hydrological cycle in AGCMs is done using continental hydrological systems (CHSs) composed of land surface models (LSMs), which provide the lower boundary conditions for heat, momentum and mass. Some AGCMs go further and include river routing models (RRMs) which are used to convert the runoff simulated by the LSMs into river discharge. RRMs transfer the continental freshwater into the oceans at specific locations (as source terms for the ocean model component). The evaluation of LSM-RRM systems is therefore a crucial task. This is generally done using offline simulations driven by atmospheric forcing which is as realistic as possible. Such forcing data are usually generated using a combination of atmospheric model reanalysis or short term forecasts combined with satellite-based products which are calibrated or bias corrected using gauge data (Dirmeyer et al., 2006; Sheffield et al., 2006; Kim et al., 2009). These simulations are then evaluated with in situ river discharge data, which does not guarantee that the spatiotemporal distribution of water storage over and under the land surface is well represented. Over West Africa especially, measurement data are difficult to access due to geographical, geopolitical and economic issues. In this context, satellite remote sensing techniques (Alsdorf and Lettenmaier, 2003; Alsdorf et al., 2007; Wigneron et al., 2003; Grippa et al., 2004) have become useful tools for hydrologic investigations. For instance, efforts have already been done to quantify the soil water content/groundwater using satellite data (Rodell et al., 2009; Grippa et al., 2011). Satellite altimetry has also been used for systematic monitoring of water levels in large rivers, lakes and floodplains and several studies have demonstrated the capability of using these sensors locally for estimating river discharge in large rivers, including the Amazon River (Leon et al., 2008; Calmant et al., 2008; Getirana et al., 2010), the Ganges-Brahmaputra (Papa et al., 2010a) or the Lake Chad basin (Coe and Birkett, 2004). Also, an advanced study of satellite altimetry by Enjolras and Rodriguez (2009) intended to derive water surface elevation of narrow river channels by using likelihood-estimation problem. In parallel, globally applicable remote sensing technique employing a suite of satellite observations has been developed and now provides estimates of the spatial and temporal dynamics of surface water extent at the global scale over the last 2 decades (Prigent et al., 2001, 2007; Papa et al., 2010b). In the future, the joint CNES-NASA Surface Water Ocean Topography (SWOT, to be launched in 2020) mission will measure the surface water height with an unprecedented resolution of 50 m over the globe (Alsdorf et al., 2007; Rodriguez, 2009). This will enable a global scale near real time monitoring of the majority of the worlds rivers, lakes and reservoirs with spatial resolution of about one hectare (Lee et al., 2010; Biancamaria et al., 2010). Such data should significantly accelerate the improvement of the representation of hydrology for global scale models.

The need for a better representation of the global water budget has resulted in numerous implementations of river routing schemes into LSMs, and they vary widely in their complexity and degree of calibration. For water management applications on the watershed scale, highly parameterized, geographically specific models can be used to provide accurate estimates of streamflow and reservoir status (Zagona et al., 2001; Dai and Labadie, 2001; Habets et al., 2008). For global scale applications, however, computationally efficient, easily parameterized, comparatively simple and physically-based routing methodologies are preferable. In fact, land waters are supposed to play an important role in the atmosphere and ocean dynamics (Alkama et al., 2008; Dirmeyer, 2000, 2001; Douville, 2000, 2003, 2004; Gedney et al., 2000; Koster et al., 2000, 2002; Lawrence and Slater, 2007; Molod et al., 2004). In AGCM applications, it is most important to close the water budget and get a good representation of the fluxes of water into the atmosphere and ocean. An early influential effort at large scale routing was done by Vorosmarty et al. (1989) who prepared a river routing network for the Amazon basin at a 0.5° resolution. Runoff produced by a water balance approach was routed through the network using a linear transfer model, with flow time calculated as a function of flow length, estimated subgrid scale sinuosity, and grid scale

velocities estimated on the basis of mean downstream discharge (Leopold et al., 1964). A similar linear transfer model was adopted by Miller et al. (1994) for application within the Goddard Institute for Space Studies (GISS) General Circulation Model (GCM) at the global scale. In their formulation, runoff produced by a GCM at $4^\circ \times 5^\circ$ was routed to the ocean through a $2^\circ \times 2.5^\circ$ network in which flow direction was determined by topography and velocity was a function of the slope. Because the scale of the implementation was quite coarse, slope based estimates of velocity were intentionally calculated to yield low values, providing an implicit correction for subgrid scale sinuosity and the time it would realistically take runoff to work its way through the river system. Sausen et al. (1994) implemented a linear routing scheme for the European Center Hamburg (ECHAM) GCM, with transport parameters semi-objectively calibrated to match observed flow in major gauged rivers. In a study of the Amazon River system, Costa and Foley (1997) adopted the velocity estimation procedure of Miller et al. (1994). As a refinement, they estimated the sinuosity coefficient independently for each tributary within the Amazon basin, and they adjusted velocities as a function of stream order. Costa and Foley (1997) further divided runoff into surface and subsurface components and applied differential source retention times to each. Further variants on the Miller et al. (1994) approach include the global hydrological routing algorithm (HYDRA, Coe, 2000), which was implemented at a 5° resolution and included variability in surface waters, and made some adjustments to the Miller et al. (1994) method for calculating distributed velocities. Oki and Sud (1998) and Oki et al. (1999) continued this line of application through the development of the topographically corrected integrating pathways for routing models, TRIP (Total Runoff Integrating Pathways). Arora and Boer (1999) implemented a time-evolving velocity that depends on the amount of runoff generated in the GCM land grid, using Mannings equation to estimate flow velocities for a river chanel with a rectangular section.

Decharme et al. (2008, 2011) used the TRIP approach to implement a flood routing scheme into the ISBA (Interaction Soil Biosphere Atmosphere)-TRIP CHS. The scheme accounts explicitly for the river routing, precipitation interception by the floodplains, the direct evaporation from the free water surface, and the possible re-infiltration into the soil in flooded areas. The regional and global evaluations of this scheme at a 1° by 1° spatial resolution emphasized the importance of floodplains in the continental part of the hydrologic cycle, through generally improved river discharges and a non-negligible increase of evapotranspiration. However, it was noticed that over some basins, including the Niger, the discharge was still overestimated (Decharme et al., 2011). A possible identified cause was that these regions might overlie large aquifers that can be relatively uncoupled to the river.

The difficulty of modelling the Niger basin and the current concerns about water resource management in West Africa make the improved understanding of this basin a scientific and socio-economic challenge. Moreover, its role in climate change and its potential feedback with atmosphere are crucial issues. It is then important for a LSM to be able to reproduce the key components of the water cycle and their evolution which will enable the detection of big anomalies in climatologic applications. The purpose of this study is to evaluate the performance of the ISBA-TRIP CHS model, including a flooding scheme and a new simple aquifer reservoir, over the Niger basin using comparisons with in situ measurements as well as recently available satellite derived data from 2002–2007. This period covers the core observation period of the African Monsoon Multidisciplinary Analyses (AMMA) project (Redelsperger et al., 2006). More precisely, the model is run in 4 different configurations (with/without flooding scheme/aquifers) to evaluate the impact of floods and aquifers on the Niger basin model configuration.

In this study, we first examine the routing scheme and its ability to simulate discharge simulated by LSMs from the AMMA Land surface Model Intercomparison Project (ALMIP). For this, TRIP was run in offline mode (default made with no feedbacks with LSMs) with total runoff from 11 LSMs, including ISBA, as input data in order to explore the impact of routing alone on the river discharge. Secondly, we evaluate the ISBA-TRIP CHS model in fully coupled LSM-RRM mode in four different configurations using two rainfall datasets. The evaluation is done using a large variety of data consisting of gauging measurements for discharge and satellite-based products, such as water heights and flooded areas. The study also attempts to give quantitative estimates of the contribution of the different water budget components over the basin using satellite data. In Sect. 4, sensitivity tests were performed to determine the robustness of the model and where the greatest uncertainties exist with respect to model parameters. Finally, conclusions and perspectives are given in Sect. 5.

2 The ISBA-TRIP model

2.1 Review of the ISBA-TRIP model

ISBA is a state-of-the-art land surface model which calculates the time evolution of the surface energy and water budgets (Noilhan and Planton, 1989). In this paper, we use the 3-layer force-restore option (Boone et al., 1999). It includes a comprehensive sub-grid hydrology to account for the heterogeneity of precipitation, topography and vegetation in each grid cell. A TOPMODEL approach (Beven and Kirkby, 1979) has been used to simulate a saturated fraction, f_{sat}, where precipitation is entirely converted into surface runoff (Decharme et al., 2006). Infiltration is computed via two sub-grid exponential distributions of rainfall intensity and soil maximum infiltration capacity (Decharme and Douville, 2006).

The TRIP RRM was developed by Oki and Sud (1998) at the University of Tokyo. It was first used at Météo-France to convert the model simulated runoff into river discharge using a global river channel network at a 1° resolution. The original TRIP model is only based on a single surface prognostic reservoir, S (kg), whose discharge is linearly related to the river mass using a uniform and constant flow velocity.

In the ISBA-TRIP CHS, TRIP takes into account a simple groundwater reservoir, G (kg), which can be seen as a simple soil-water storage, and a variable stream flow velocity computed via the Mannings equation (Decharme et al., 2010; Appendix A). In addition, ISBA-TRIP includes a two-way flood scheme in which a flooded fraction, f_{flood}, of the grid cell can be determinated (Decharme et al., 2008, 2011). The flood dynamics are described through the daily coupling between the ISBA land surface model and the TRIP river routing model, including a prognostic flood reservoir, F (kg). This reservoir fills when the river height exceeds the critical river bankfull height, h_c (m) (Appendix B). The flood interacts with the soil hydrology through infiltration, I_f (kg s^{-1}), with the overlying atmosphere through precipitation interception P_f (kg s^{-1}), and through free water surface evaporation E_f (kg s^{-1}). These three terms are calculated by multiplying, respectively, the total infiltration, precipitation interception and water surface evaporation over the grid cell by the ratio of flooded area to the grid area. This results in a system of three prognostic equations:

$$\left|\begin{array}{l} \frac{\partial G}{\partial t} = Q_{sb} - Q^G_{out} \\ \frac{\partial S}{\partial t} = Q^S_{in} + Q^G_{out} + \left(Q^F_{out} - Q^F_{in}\right) - Q^S_{out} \\ \frac{\partial F}{\partial t} = Q^F_{in} + (P_f - I_f - E_f) - Q^F_{out}, \end{array}\right. \quad (1)$$

where Q_{sb} (kg s^{-1}) is the deep drainage from ISBA, Q^G_{out} (kg s^{-1}) the groundwater outflow, Q^S_{in} (kg s^{-1}) the sum of the surface runoff from ISBA within the grid cell with the water inflow from the upstream neighboring grid cells, and Q^S_{out} (kg s^{-1}) is the simulated discharge, while Q^F_{in} and Q^F_{out} (kg s^{-1}) represent the flood inflow and outflow, respectively. See Appendix A and B for more details.

The global evaluation of the ISBA-TRIP CHS model at a 1° by 1° resolution suggested that the model may not take into account some important process such as the presence of large aquifers in certain regions (Decharme et al., 2011). Also, by comparing the chemical composition of river water and groundwater, Fontes et al. (1991) demonstrated that significant aquifer recharge occurs in the Niger Inland Delta region, especially during summer flooding. For these reasons, a simple linear aquifer reservoir was added to the model. This reservoir was built on the example of the groundwater reservoir, G, but with a significantly longer time delay factor, τ_{aq} (s). This results in a new system of four prognostic equations:

$$\left|\begin{array}{l} \frac{\partial G}{\partial t} = \alpha Q_{sb} - Q^G_{out} \\ \frac{\partial S}{\partial t} = Q^S_{in} + Q^G_{out} + \left(Q^F_{out} - Q^F_{in}\right) - Q^S_{out} \\ \frac{\partial F}{\partial t} = Q^F_{in} + (P_f - I_f - E_f) - Q^F_{out} \\ \frac{\partial Aq}{\partial t} = (1 - \alpha)\, Q_{sb} - Q^{Aq}_{out}, \end{array}\right. \quad (2)$$

where α represents the fraction of deep drainage going into the groundwater reservoir while the rest of the drainage $(1-\alpha)$ goes into the aquifer. Unlike the groundwater reservoir, we assume that the aquifer reservoir local feedbacks are negligible, but contribute to the flow at the mouth of the river. The aquifer outflow Q^{Aq}_{out} (kg s^{-1}) can be written as follows:

$$Q^{Aq}_{out} = \frac{Aq}{\tau_{Aq}}, \quad (3)$$

where τ_{Aq} (s) is a constant and uniform time delay factor, which represents the characteristic timescale for the aquifer reservoir to drain laterally to the ocean (out of the basin). This simple approach is currently motivated mainly by the lack of data describing the water table, which would be required for a more detailed approach. Figure 1 illustrates the configuration of the ISBA-TRIP CHS model used in this study.

2.2 TRIP specific parameters

The baseline parameter values are presented in this section; the sensitivity of the model to these parameters will be investigated in a subsequent section. For the model evaluation, the time delay parameters for the groundwater and deep aquifer reservoirs are fixed to 30 days and 4 yr, respectively. The aquifer parameter α is initially fixed at 3/4 (which implies that 1/4 of the drainage flows into the deep aquifer). The aquifer reservoir is defined equally in each pixel.

The river width is an important parameter because it modulates both the river flow speed and the floodplain dynamics. It is computed over the entire TRIP network via an empirical mathematical formulation that describes a simple geomorphologic relationship between W and the mean annual discharge at each river cross section (Knighton, 1998; Arora and Boer, 1999; Moody and Troutman, 2002; Decharme et al., 2011):

$$W = \max\left(30,\ \beta \times Q^{0,5}_{yr}\right), \quad (4)$$

where $Q^{0,5}_{yr}$ (m^3 s^{-1}) is the annual mean discharge in each grid cell estimated using the global runoff database from Cogley (1979). As discussed in Decharme et al. (2011), the β coefficient can vary drastically from one basin to another (Knighton, 1998; Arora and Boer, 1999; Moody and Troutman, 2002). Decharme et al. (2011) proposed that β varies according to climatic zone and fixed β to 20 for monsoon

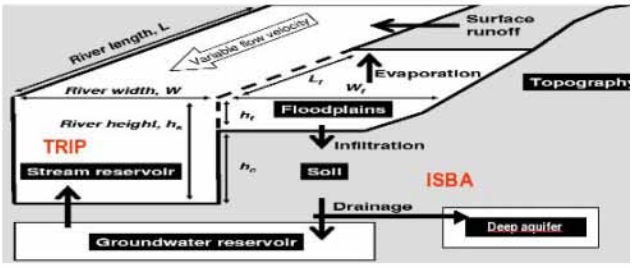

Fig. 1. Schematic representation of the ISBA/TRIP (Oki et al., 1999; Decharme, 2007) coupled system. The surface runoff calculated by the land surface model (ISBA) flows into the stream reservoir. The flood dynamic is described using a prognostic flood reservoir which fills when the river height exceeds a critical value and vice versa. The flood fraction is based on sub-grid topography. Finally, we add a linear aquifer reservoir so that the deep drainage is divided between the groundwater and the deep aquifer reservoirs.

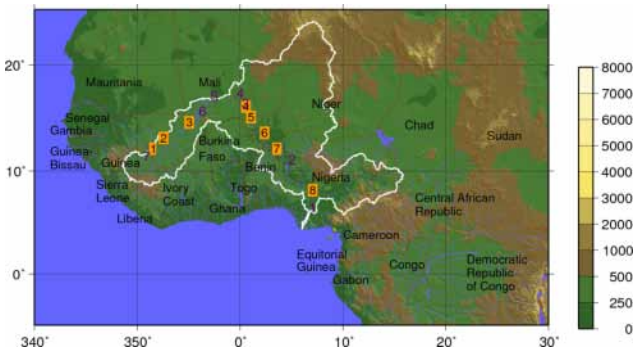

Fig. 2. ALMIP domain (stops at latitude 20° N). The spacial resolution is 0.5° × 0.5°. The white contour is the delimitation of the Niger basin. The yellow squares are the stations where discharge observations are available: (1) Banankoro (2) Koulikoro (3) Ke Macina (4) Niamey (5) Ansongo (6) Kandadji (7) Malanville (8) Lokoja. The purple figures are the sites where height change observations are used for evaluation. The legend indicates the topographical heights values (m).

basins and to 13 for semi-arid and arid basins. As the Niger river flows through both such climate zones, two different values are used within the Niger basin: β is 20 for the branch of the river going from the river mouth (5° N) to 12° N and β is fixed to 10 for the remaining branch of the river. The spatial distribution of the river width is shown in Fig. 3a.

The key parameter for the floodplain parameterization is h_c, the critical river bankfull height (Decharme et al., 2008, 2011). In this study, as proposed by Decharme et al. (2011), it is computed according to the river width via a simple power function:

$$h_c = W^{1/3} . \quad (5)$$

The spatial distribution of h_c is shown in Fig. 3b. However, owing to both the uncertaintities in this parameter and its impact on model results, sensitivity tests will be carried out using arbitrary $h_c \pm 20\,\%$ (Decharme et al., 2008), leading to an increase or decrease in bankfull height up to 2 m.

Finally, as in Decharme et al. (2010), the Manning friction factor n_{riv} varied linearly and proportionally to W from 0.04 near the river mouth to 0.1 in the upstream grid cells (Fig. 3c):

$$n_{riv} = n_{min} + (n_{max} - n_{min}) \left(\frac{W_{mouth} - W}{W_{mouth} - W_{min}} \right), \quad (6)$$

where n_{riv} represents the Manning n factor of the grid cell, n_{max} and n_{min} the maximum and the minimum values of the Manning friction factor (respectively equal to 0.1 and 0.04), W_{min} (m) the minimum river width value and W_{mouth} (m) the width of the mouth in each basin of the TRIP network.

3 Model setup and experimental design

3.1 Methodology

In order to determine the impact of the flooding scheme on simulated discharges, the TRIP routing model is used in offline mode, uncoupled from a LSM and without floodplains. ALMIP I, which is a part of the AMMA project, was motivated by an interest in fundamental scientific issues and by the societal need for improved prediction of the West African Monsoon (WAM) and its impacts on West African nations (Redelsperger et al., 2006). As part of this project, ALMIP I focused on better understanding land-atmosphere and hydrological processes over Western Africa (Boone et al., 2009). LSMs were run offline with prescribed atmospheric forcing consisting in a combination of observations, satellite products and atmospheric model output data. All of the LSMs used the same computational grid at a 0.50° spatial resolution (see the domain on Fig. 2). The advantage of using ALMIP data is that each LSM can simulate a different runoff response, therefore we use an ensemble of inputs. In the current study, 11 simulations are used over the 2002–2007 period. TRIP is used to compute daily outputs of discharges along the river and water mass storage for each activated reservoir.

In addition, the ISBA-TRIP CHS coupled model is used with and without the flooding scheme to quantify the impact of the scheme on the discharge and the surface energy budget. As the TRMM-3B42 rainfall (see next section for details) was used as forcing for the ALMIP experiment, the same forcing is used for the ISBA-TRIP CHS simulation with and without the flooding scheme. In the second part of this study, the deep aquifer reservoir is implemented into the ISBA-TRIP CHS model and deep drainage water is then distributed between deep soil layers and this aquifer reservoir

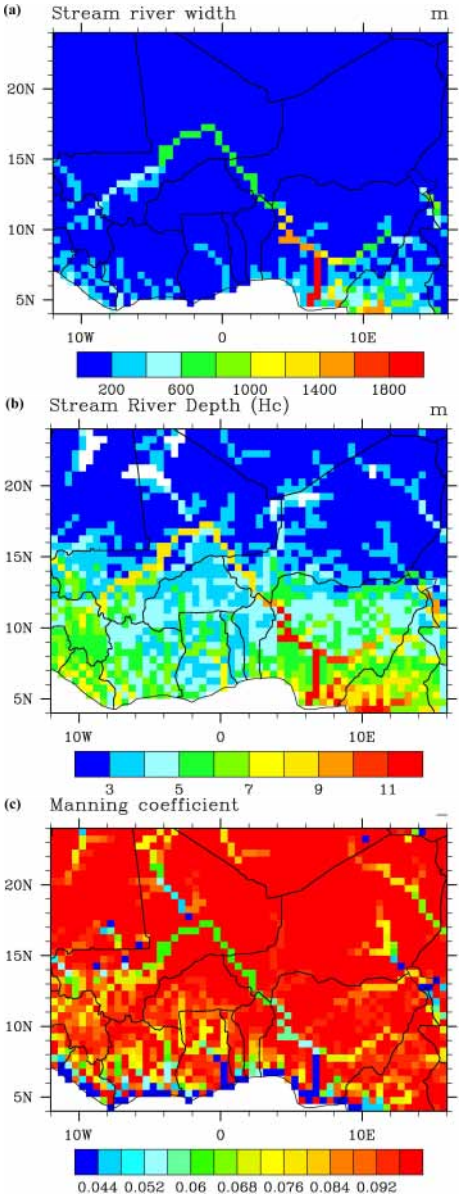

Fig. 3. Some TRIP parameters. Spatial distribution of the river width (up left), the river depth (up right) and the Manning coefficient (down).

(see details in Sect. 2). We then evaluate the ISBA-TRIP CHS model in four different configurations:

- no flooding scheme and no aquifer reservoir (NOAQNF);
- flooding scheme activated, no aquifer reservoir (NOAQF);
- no flooding scheme, insertion of aquifer reservoir (AQNF);
- flooding scheme activated, insertion of aquifer reservoir (AQF).

The model is run using two rainfall datasets (see next section for details) to take rain uncertainty into account in a simple manner, leading to 8 different simulations. Comparison with both in situ and remote sensing data will allow us to evaluate the simulated surface processes, the impact of the inclusion of floodplains and aquifers, and the ability of the model to estimate the river discharge.

3.2 Atmospheric forcing dataset to run ISBA-TRIP

The atmospheric state variables are based on the European Centre for Medium Range Forecasts (ECMWF) ECMWF numerical weather prediction (NWP) model forecasts for the years 2002–2007. The forcing variables consist in the air temperature, specific humidity, wind components at 10 m, and the surface pressure, all at a 3 h time step. Because of the importance of having accurate incoming radiation fluxes and precipitation, and because of the potentially significant errors in these variables derived from NWP models over this region (e.g. see Boone et al., 2009), merged satellite products are used. The downwelling longwave and shortwave radiative fluxes are provided by the LAND-SAF project (Geiger et al., 2008). Two products are used for rainfall forcing. The TRMM 3B42 product (Huffman et al., 2007) is used by default.

However, several studies have shown that RFE2 (Laws et al., 2004) produces rainfall over the Sahel agrees better with observed values than the other available rainfall products (e.g. Pierre et al., 2011), but it is at a time step which is not well adapted to land surface modelling (daily time step). Therefore, a second set of rainfall forcing data was created by disaggregating the daily RFE2 to a three hour timestep using the TRMM rainfall data. The monthly total RFE2 rainfall is well preserved using this simple downscaling method. This rain forcing is referred to as RFE-Hybrid (RFEH) herein. All of the simulations presented in this paper were done using the two datasets as forcing rainfall.

3.3 Evaluation datasets

Over the evaluation period (2002–2007), the simulated discharges are compared with daily gauge measurements along the Niger river from the Niger Basin Authority (ABN) as part of their Niger-HYCOS Project. These data are available in Koulikoro, Banankoro, Ke-Macina, Kandadji, Niamey, Ansongo, Malanville and Lokoja (see Fig. 2).

Satellite-derived inundation estimates are used to evaluate the spatial distribution and the time evolution of the flooded areas. Two different products are used. The first product is based on data from the MODIS multispectral imaging system installed onboard the Terra and Aqua satellites. In this study, the surface reflectance product (MOD09GHK) is used, which is defined as the reflectance that would be measured at the land surface if there were no atmosphere. The spatial resolution is 500 m for the corresponding MODIS images and

the coverage is global (Vermote et al., 2002). In order to detect open water and aquatic vegetation in arid and semi arid regions, a classification is performed using the fact that water surfaces do not reflect in the visible and near infra-red part of the spectrum. A threshold value has been estimated for reflectance in the MODIS frequency band-5 1230–1250 nm and for the NDVI index (Table 1) in order to delineate the shallow, sediment laden, and open water over the Inner Niger Delta, and also in order to distinguish between aquatic vegetation and vegetation on dry land. It has been assumed that small values of surface reflectance in band-5 characterize open water, independent of the NDVI index. When the surface reflectance in band-5 increases to the median value, depending on the NDVI index, it is assumed that there is a partial coverage of dry land by water, aquatic vegetation or vegetation on dry land. Finally, dry land is assumed when the NDVI is small and surface reflectance in band-5 is large. NDVI has been shown to be a robust index for monitoring temporal changes of the vegetation photosynthetic activity (Lyon et al., 1998; Lunetta et al., 2006). In the arid environment, a high level of vegetation photosynthetic activity can only be sustained by the presence of surface water or groundwater discharge. If dense enough, the aquatic vegetation and hydrophilic plants can mask underlying water and should be included in the estimate of the total area of the floodwaters. The NDVI ranges from negative values (open water) to >0.5 for dense vegetation.

The second product consists in global estimates of the monthly distribution of surface water extent at about 25 km sampling intervals. These data were generated from complementary multiple satellite observations, including passive (Special Sensor Microwave Imager) and active (ERS scatterometer) microwaves along with visible and near infrared imagery (advanced very high resolution radiometer; AVHRR). These estimates were first developed over 1993–2000 (Prigent et al., 2007), adjusted and extended over 1993–2004 (Papa et al., 2010b) and recently recomputed for the entire period 1993–2007. This dataset has been extensively evaluated at the global scale (Papa et al., 2010b) and at river basin scale, including the Niger river (Papa et al., 2008). In the present study, this dataset is aggregated to a 0.5° resolution and referred to as PP. Because PP does not distinguish between the diverse anthropogenic and/or natural water bodies, while the ISBA-TRIP output must be compared only with flooded areas, two additional datasets are used to hybridize PP in order to conserve information on flood inter-annual variability only: the Global Lakes and Wetland Database (GLWD; Lehner and Döll, 2004) and the Monthly Irrigated and Rainfed Crop Areas (MIRCA2000; Portmann et al., 2010) database. The corresponding final product is named CPP in this study. The methodology is described in detail by Decharme et al. (2011), and so it is not detailed here.

Water height changes over the basin are evaluated using the HYDROWEB hydrological database (http://www.legos.obs-mip.fr/en/equipes/gohs/resultats/i_hydroweb). The water level time series are based on altimetry measurements from ENVISAT satellite. Seven sites were chosen for the evaluation, one upstream of the Niger inner delta, four downstream of the delta and two in the delta. The data are available at a regular 35 days time step (with occasional missing data) from November 2002 to the end of 2007 (Calmant et al., 2008).

Total Water Storage (TWS) variations over the entire basin are evaluated using data from the Gravity Recovery and Climate Experiment (GRACE; Tapley et al., 2004). GRACE provides monthly TWS variation estimates based on highly accurate maps of the Earth's gravity field at monthly intervals at a resolution of approximately 300–400-km (Wahr et al., 2004; Swenson et al., 2003). The instrumentation and onboard instrument processing units are described in detail in Haines et al. (2003). Here, we used 60 months (from January 2003 to December 2007, excluding June 2003 and January 2004 because products are not available) of the Release 04 data produced by the Center for Space Research (CSR at The University of Texas in Austin), the Release 4.1 data produced by the Jet Propulsion Laboratory (JPL), and the GeoForschungsZentrum (GFZ) Release 04 (more details concerning GRACE data are available online at http://grace.jpl.nasa.gov/data/). The combination of these data with those datasets described in the previous paragraphs above will allow us to evaluate the distribution of water in the different TRIP reservoirs and to have a first estimation/validation of the aquifer water storage variations.

4 Results

4.1 Improvement of simulated discharges due to river flooding

The evaluation of the simulated river discharge is important for hydrological applications as well as for climate studies. Previous studies (Bonan, 1995; Coe et al., 2008; Decharme et al., 2008, 2011; Alkama et al., 2010; Dadson et al., 2010) have shown that the inclusion of a flooding scheme can impact the hydrological cycle by increasing the average evaporation and reducing the simulated discharge, which leads to a better estimation of the latter. Indeed, while an increasing number of LSMs used for large scale hydrological or GCM applications use river routing, most of these models do not represent floodplains. Flooded zones can be significant sources of evaporation and have a role of surface water storage, and their exclusion can result in an overestimation of the discharge for basins with significant annual flooding. To generalize this result, the TRIP RRM model was used in offline mode and without the flooding scheme (or aquifers) to convert simulated runoff and drainage from 11 LSMs into discharge. The LSMs considered for this study were part of the ALMIP I project (Boone et al., 2009). The Fig. 4 shows

Table 1. Threshold values used for the classification surface type used to monitor flood events. Band unit of reflectance is internal HDF-EOS data format specific to the Modis data and do not correspond to usual reflectance unit.

	Open water	Mix water/Dry land	Aquatic vegetation	Vegetation	Dry land
Band 5	<1200	>1200 & <2700	>1200 & <2700	>2700	>2700
NDVI	No test	<0.4	>0.4	>0.4	<0.4

the mean daily discharges simulated by the ALMIP models (black line) for several locations along the river. The blue range is the difference between the minimum and the maximum value of discharges simulated by the models and the red line is the observed discharge. The corresponding statistics are given in Table 2. Due to the bias in precipitations for years 2005 to 2007 (discussed in Sect. 4.4.), the statistics are calculated from 2002 to 2004 in order to better reflect the model performance.

In terms of observed discharge, there is a clear change of behaviour after the delta (Niamey, ansongo, Kandadji, Malanville, Lokoja) compared to upstream of the delta (Banankoro, Koulikoro, Ke Macina). Indeed, the discharge before the delta is almost twice higher than downstream of the delta. This reflects the significant impact of the inner delta on the discharge amplitude due to the floodplains. The first 3 discharges on the Fig. 4 are located before the inner delta area (Banankoro, Koulikoro and Ke Macina). For these three locations, the discharge is reasonnably represented by the ALMIP models. A bias in discharge is observed in 2005, 2006 and 2007 where the models simulate a smaller discharge compared to the previous years. This can be due to a bias in the rain forcing and will be discussed in Sect. 4.4. However, for the sites located downstream of the inner delta area (Niamey, Kandadji, Ansongo, Malanville and Lokoja) all of the ALMIP land surface models clearly overestimate the discharge leading to poor results compared to the three locations before the inner delta (see Table 2). In Malanville, the mean simulated discharge is around 5 times higher than that observed over this period. At the other sites (Niamey, Kandadji, Ansongo, and Lokoja), the mean simulated discharge is 2 to 2.8 times higher than observed. However, the variability of the discharge is generally well captured by the models as pointed out by the correlation scores (see Table 1). The green line represents the discharge simulated by the ISBA-TRIP CHS model with the flooding scheme activated. The results can be seperated into three classes. Fisrt, in Banankoro and Koulikoro (before the inner delta), the discharge and thus the scores are not significantly changed, probably because no floods occur in these places. Second, after the inner delta (Niamey, Ansongo, Kandadji, Malanville and Lokoja), discharge has decreased considerably (50 %) in Niamey, Kandadji, Ansongo and Malanville and 26 % in Lokoja. The root mean square error (rms) has decreased considerably compared to the simulation without flooding scheme (see Table 2). Indeed, part of the water in the floodplains evaporates, while part infiltrates into the flooded soil thereby reducing the stream reservoir water storage and discharge. The Nash-Sutcliffe coefficient or efficiency (eff) is also improved. Finally, in Ke Macina, the discharge is deteriorated by the addition of the flooding scheme. Among the sites before the inner delta, Ke Macina is the closest to the delta. It is likely that the model floods occur too soon upstream of the delta. This can be directly linked to a poor parametrisation or model parameter value (such as the river width) in this particular area. In the 3 locations upstream of the delta, there is a significant decrease of the simulated discharge in 2005, 2006 and 2007 which is not observed. This reduction of the discharge is observed for all the LSMs as well as for both configurations of ISBA-TRIP (with and without floods) and is more likely to be due to rainfall errors. This issue will be discussed in Sect. 4.4.

The impact of the flooding scheme on the surface energy budget was also investigated where the total evaporation includes evaporation from the soil and flooded areas and transpiration. The flooding scheme contributes to an increase in the evaporation mainly over the inland delta and in the southern part of the basin (+280 % with TRMM rainfall and +200 % with RFEH), which are areas which generally experience significant floods (see Sect. 4.2.2).

According to these results the floods occurring in the Niger inner delta region have an impact on the discharge, which is characterized by a decrease in its amplitude. The in situ discharge is among twice higher before the delta than after (Niamey, Ansongo, Kandadji and Malanville) and increases again when reaching the mouth of the river (Lokoja) where several tributaries join the Niger river. In addition, the flooding scheme allows a better simulation of the discharge after the delta, highlighting the importance of representing floodplains in LSMs. However, some model deficiencies remain, such as a bias of discharge in Ke Macina (possibly due to the previous cited reason), but also a bad reproduction of the recession flow during the dry season. In fact, the discharge remains relatively high during the dry season compared to the observations, which implies that there is too much water in the river. Several reasons for this can be identified, such as underestimated evaporation, an underestimation of the water in flooded areas or the neglect of aquifers. Anthropologic activities (dams, agriculture and water use for domestic consumption) are not explicitly accounted for and can also explain the bias between observed and simulated discharge, especially during the dry season when the population

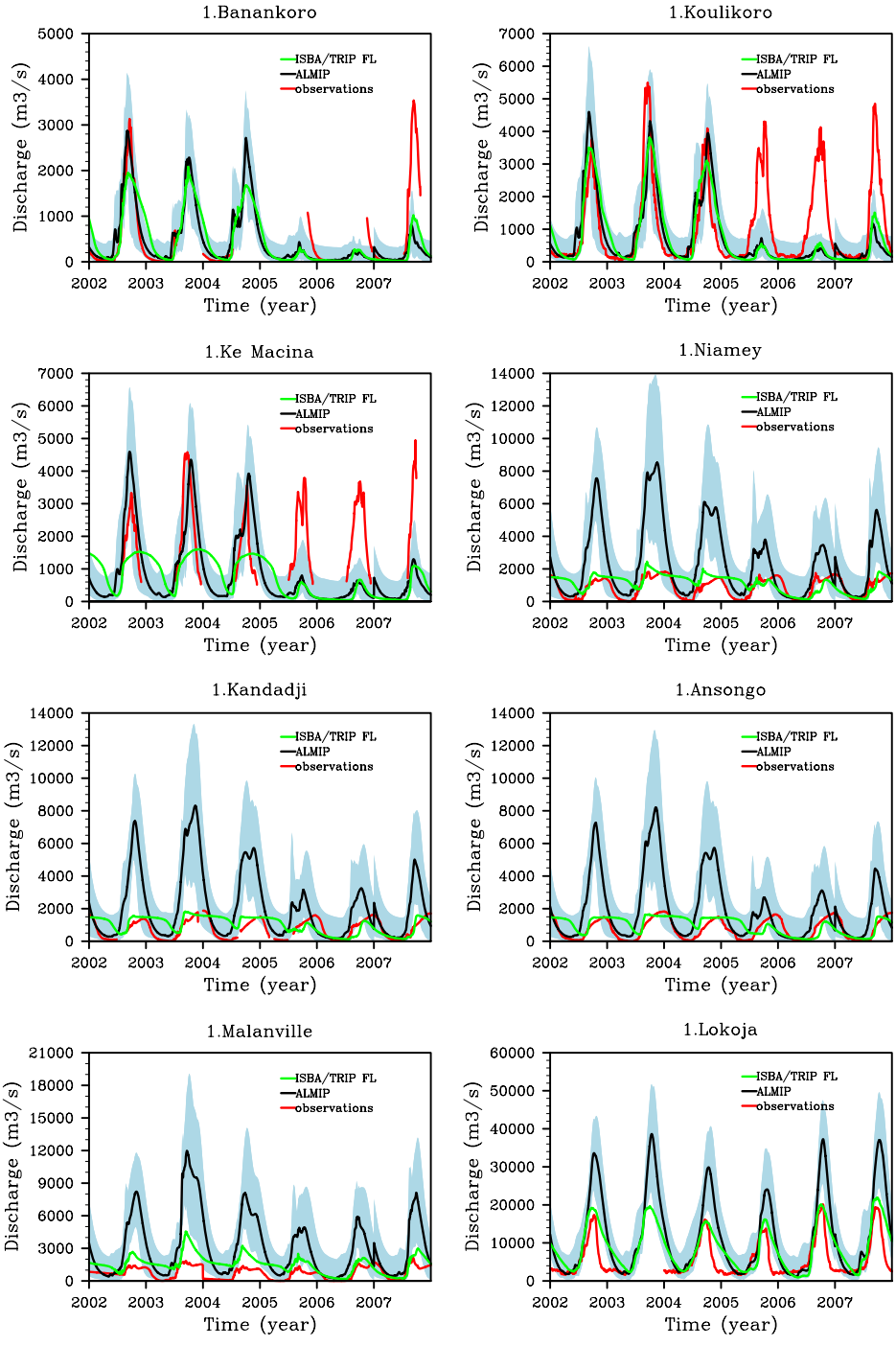

Fig. 4. Daily discharges (2002–2007) simulated by ALMIP LSMs without floods (average, black line) and by ISBA-TRIP using the flooding scheme (green). Observations are in red and the blue range is limited by the minimum and maximum discharge simulated by LSMs. The TRMM-3B42 rain product is used as forcing input.

might need to extract more water from the river due to the lack of rain. In order to investigate the impact of aquifers on the discharge, a relatively simple and linear aquifer reservoir was added to the model (see Sect. 2.1 for details). The next section will focus on 4 different configurations of the ISBA-TRIP model and their respective impacts on some variables involved in the water cycle (discharge, water level changes, flooded fraction and total water storage). In order to take into account the rain uncertainties, two rainfall dataset are used as forcing (see Sect. 3.2 for details).

Table 2. Daily statistic scores of the discharge for the ALMIP LSMs and ISBA/TRIP with and without flooding from 2002 to 2004. TRMM-3B42 is used as forcing.

Corr.	Ban	Kou	KeM	Nia	Ans	Kan	Mal	Lok
ALMIP	0.97	0.83	0.5	0.8	0.73	0.73	0.82	0.78
ISBA−TRIP NF	0.98	0.9	0.7	0.76	0.73	0.74	0.75	0.81
ISBA−TRIP F	0.86	0.86	0.23	0.59	0.56	0.58	0.69	0.82
NS								
ALMIP	0.9	0.63	−0.2	−23.32	−23	−19.31	−62.42	−2.95
ISBA−TRIP NF	0.81	0.57	−0.95	−24.6	−22.9	−23.07	−57.08	−2.27
ISBA−TRIP F	0.69	0.7	−0.34	−0.52	−0.91	−0.37	−4.42	0.02
RMS								
ALMIP	0.58	0.76	0.6	3.54	4.04	3.61	5.25	1.66
ISBA−TRIP NF	0.81	0.81	0.76	3.63	4.36	3.93	5.03	1.51
ISBA−TRIP F	1.04	0.68	0.63	0.89	1.14	0.94	1.54	0.83

4.2 Separate impact of floods and aquifers on the Niger basin

4.2.1 Discharge

A fourth reservoir was added to the ISBA-TRIP model to represent deep aquifer processes (Sect. 2). This reservoir is supplied by a fraction of the soil drainage and it does not supply water back the river. Indeed, the model simulates too much water in the river, which could be due to the presence of large aquifers (Fontes et al., 1991; Decharme et al., 2011). Different values of the aquifer recharge factor (1-α) were tested and only the most relevant result is kept for the evaluation (see sensitivity tests in Sect. 4.6 for further details). In order to better understand the separated impacts of aquifers and floods, four different configurations of the model are tested in this study:

- no flooding scheme and no aquifer reservoir (NOAQNF);
- flooding scheme activated, no aquifer reservoir (NOAQF);
- no flooding scheme, insertion of aquifer reservoir (AQNF);
- flooding scheme activated, insertion of aquifer reservoir (AQF).

Two different rainfall datasets are also used as forcing: TRMM-3B42, already used in the ALMIP I project and in the previous section; and RFEH (see Sect. 3.2).

Figure 5 shows the simulated discharge for the 4 configurations when the model is forced by TRMM-3B42 and RFEH, respectively. Table 3 presents the statistical scores for each configuration and the best scores are in bold type. The statistics are generally better when both floods and aquifers are represented in the model, especially downstream of the inner delta when the model is forced by TRMM-3B42 (see Table 3). Upstream of the delta, the Nash-Sutcliff coefficient and the RMS are generally better without aquifers with both forcing. With RFEH, the aquifers do not lead to a systematic improvement of the scores; however, they do not lead to a significant degradation either.

Before the inner delta, the introduction of aquifers impacts the discharge mostly by reducing the monsoon peak, resulting in a deterioration of the rms score. This deterioration might be due to the "simplicity" of the aquifer reservoir parametrisation. Indeed, the aquifer is homogeneously defined over all the domain and can generate biases in regions where this aquifer either does not exist or has a minor role.

Downstream of the inner delta, the aquifer impacts mostly the recession flow in two manners: it lenghtens the period of maximum discharge and reduces the low flows. This results in a deterioration of the period except in Lokoja where the period and the recession law are improved (Fig. 5a). When the model is forced by TRMM, the presence of aquifers considerably improves the recession during the dry season. The reduction of low flows is explained by the fact that the river empties faster after the rainy season which results in a more realistic discharge during the dry season. In terms of statistics, the scores (ratio, rmse, eff) are similar or slightly deteriorated, except in Malanville and Lokoja where they are improved. The correlation score, however, is improved at all of the sites. The sensitivity of the model to the choice of the time delay factor τ_{Aq} and the fraction α will be presented in Sect. 5.

The scores are greatly improved by the addition of the flooding scheme for the locations situated downstream from the inner delta. The configuration with floods and aquifers generally leads to a good improvement of the scores in the sites located after the inner delta when the model is forced by the TRMM rainfal datasets. It is less obvious when the model is forced by RFEH rainfalls. However, when the aquifers deteriorate the scores, the deterioration is therefore small compared to the improvements (see Lokoja for example) and

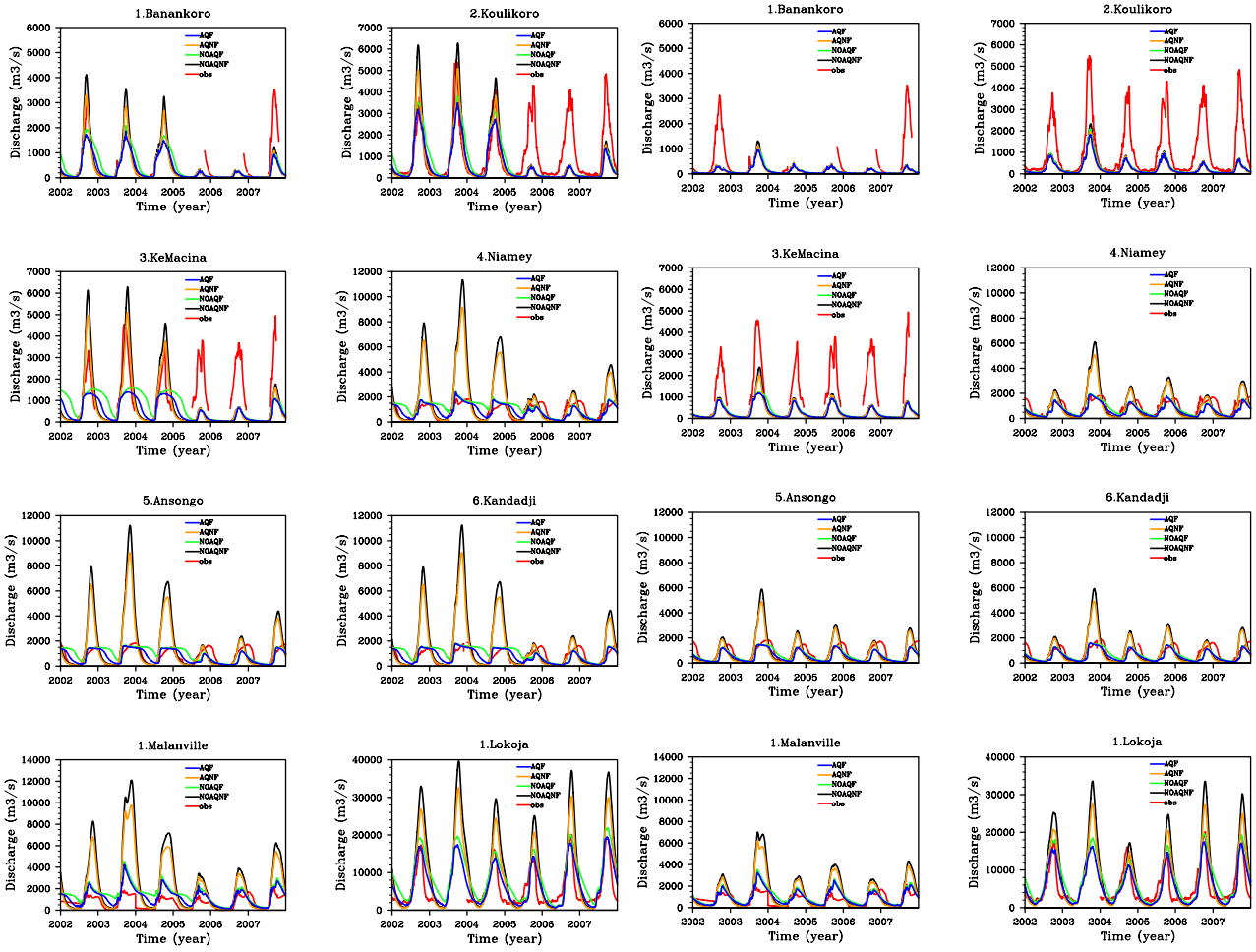

Fig. 5. Daily discharges (2002–2007) simulated by ISBA-TRIP in the 4 different configurations of the model. Observations are in red. The TRMM-3B42 (2 left columns) and RFEH (2 right columns) rain product are respectively used as forcing input.

likely due to a bad parametrisation of aquifers in these regions. However, we recall that global applications do not aim at calibrating input parameters but at detecting the key processes which impact the evolution of the water cycle. Finally, we notice that all of the configurations poorly reproduce the discharge in 2005, 2006 and (to a lesser extent) in 2007.

To investigate the role of the inner delta over evaporation, we looked at the relative difference of total evaporation over the delta [13° N–16° N; 3° W–6° W] between the simulations NOAQNF and NOAQF when the model is forced by TRMM (the results are similar withe RFEH). This is shown on Fig. 6 (blue solid line). Moreover, we added the relative difference of discharge between Niamey and Koulikoro (black solid line). Ke Macina is closer to the delta, but as many data are missing on this station, we looked at Koulikoro for the comparison. The dashed lines represent the absolute discharge in Niamey (green) and Koulikoro (red). During the monsoon, the observed discharge in Niamey is 40 to 80 % less than in Koulikoro, as noticed before. However, while the discharge in Koulikoro decreases really fast at the end of the rainy season, the discharge in Niamey remains at its maximum value and even increases a little, resulting in a second peak of discharge. While the second peak corresponds to the flood signal of the upper Niger basin delayed by the inner delta and has been observed for decades, the first peak is likely related to increased contribution of the tributaries located downstream from the delta that appeared in the recent 10 to 15 yr (Amogu et al., 2010). The transition between the monsoon and the post-monsoon regime is also visible if we look at the total evaporation simulated with and without the flooding scheme over the delta. Indeed, during the monsoon, there is hardly any difference of evaporation between the two simulations. But, during the post-monsoon, the model including floodplains simulates 30 % more evaporation than without the flooding scheme. The floodplains intensify the creation of evaporation over the delta and the time correlation with the second peak of discharge in Niamey suggest that they also have an impact on the recession flow by

Table 3. Daily statistic scores of the discharge for the 4 configurations forced by TRMM-3B42 and RFEH from 2002 to 2004.

Corr. TRMM	Ban	Kou	KeM	Nia	Ans	Kan	Mal	Lok
NOAQNF	**0.98**	0.9	0.7	0.76	0.74	0.73	0.75	0.81
NOAQF	0.86	0.86	0.23	0.59	0.58	0.56	0.7	0.82
AQNF	0.97	**0.91**	**0.74**	0.76	0.73	0.72	**0.77**	0.83
AQF	0.94	0.9	0.43	**0.81**	**0.86**	**0.83**	0.73	**0.87**
Corr. RFEH								
NOAQNF	0.9	0.88	0.79	0.71	0.65	0.66	0.74	0.82
NOAQF	0.91	0.89	0.7	0.84	0.86	0.85	0.7	0.8
AQNF	0.89	0.9	**0.82**	0.7	0.63	0.65	**0.75**	0.83
AQF	**0.92**	**0.91**	0.78	**0.84**	**0.86**	**0.85**	0.74	**0.87**
NS TRMM								
NOAQNF	0.81	0.57	-0.94	-24.62	-23.07	-26.86	-57.08	-2.27
NOAQF	0.69	0.7	-0.34	-0.53	-0.36	-0.91	-4.42	0.02
AQNF	**0.94**	**0.8**	**0.17**	-14.83	-13.88	-16.76	-35.98	-0.59
AQF	0.82	0.31	-0.43	**0.49**	**0.64**	**0.41**	**-1.97**	**0.66**
NS RFEH								
NOAQ-NF	**-0.005**	**0.25**	**-0.58**	-2.58	-2.1	-2.85	-10.17	-0.06
NOAQ-F	-0.01	0.23	-1.09	**0.69**	**0.7**	**0.71**	-0.51	0.4
AQ-NF	-0.02	-0.17	-0.81	-1.41	-1.18	-1.71	-6.31	0.48
AQ-F	-0.03	0.15	-1.19	0.64	0.63	0.69	**0.008**	**0.7**
RMS TRMM								
NOAQNF	0.81	0.81	0.76	3.63	3.93	4.36	5.03	1.51
NOAQF	1.04	0.68	0.63	0.89	0.94	1.14	1.54	0.83
AQNF	**0.46**	0.56	**0.49**	2.85	3.48	2.45	4.01	1.05
AQF	0.79	**0.56**	0.65	**0.51**	**0.63**	**0.61**	**1.14**	**0.49**
RMS RFEH								
NOAQNF	**1.88**	**1.08**	**0.69**	1.36	1.41	1.62	2.2	0.86
NOAQF	1.88	1.1	0.79	**0.4**	**0.44**	**0.44**	0.81	0.65
AQNF	1.89	1.14	0.73	1.12	1.18	1.36	1.78	0.6
AQF	1.9	1.15	0.81	0.43	0.49	0.46	**0.66**	**0.45**

lengthening the period of maximum discharge. From 2005 to 2007, we notice a weaker evaporation over the delta than during previous years. This is coherent with the simulated discharge which is also very weak during these three years.

4.2.2 Flooded areas

The quantification of wetland extent is an important step towards a better representation of surface water dynamics. In this study, the time and spatial distribution of wetlands were evaluated over the inner delta region, which is a large inundated area, and over the whole basin. Figure 7a and b show the time evolution of the mean monthly flooded fraction (in %) averaged over the inner delta region and over the Niger basin, respectively, with and without aquifers, when the model is forced by TRMM. Figure 7c and d present the same results when the model is forced by RFEH. Only the two configurations with and without aquifers are shown as there is no simulated flooded fraction without flooding scheme. The blue range on the Fig. 7a and c represents the interval between the minimum and the maximum Modis derived (JFC) flooded fraction. Over the delta, the simulated flooded fraction is generally included in this range, although it tends to be on the low end when the model is forced by

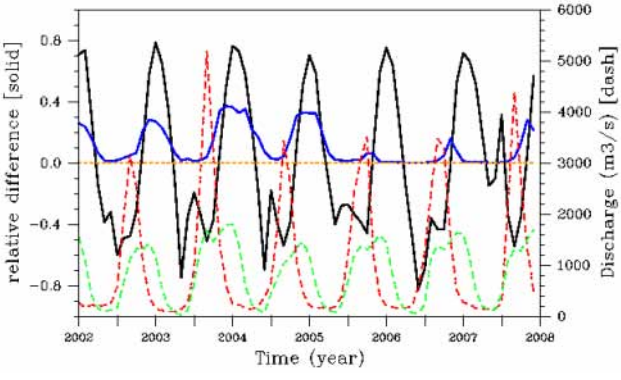

Fig. 6. Time evolution of the relative difference of simulated total evaporation between the simulation NOAQ-NF(1) and NOAQ-F(2) when the model is forced by TRMM-3B42 (solid blue line). The relative difference is the ratio $((2)-(1))/((2)+(1))$. Time evolution of the relative difference of observed discharge between Niamey and Koulikoro (solid black line). Time evolution of the discharge in Niamey (dashed green line) and Koulikoro (dashed red line).

RFEH. These results are reasonable since the Modis classification (JFC) fraction includes wetted vegetation and near-surface saturated soils. With both rainfall datasets, the presence of aquifers results in a reduction of flooded areas. But the impact of aquifers on the flooded fraction is more obvious for the simulation forced by TRMM rainfall. Indeed, the aquifers greatly improve the period of the floods. However, as shown in the figures, the CPP product is around 3 times higher than the modelled values over the basin and 10 times higher over the delta. This can be explained by the fact that the multi-satellite method can encounter some difficulties in accurately discriminating between very moist soils and standing open water, likely overestimating the actual fraction of inundations (Papa et al., 2010a, b). Model deficiencies may also explain this bias. They can be related to routing deficiencies due to a bad parametrization, or to LSMs deficiencies in the calculation of floodplains evaporation and/or infiltration.

Figure 8a and b show the time series of de-seasonalized anomalies (obtained by subtracting the 12-yr mean monthly value from individual months and then divided by the standard deviation) over the delta and over the basin, with and without aquifers, when the model is forced by TRMM. Figure 8c and d present the same results when the model is forced by RFEH. Over the delta, the Fig. 8a and c suggest that the model and the data are in good agreement in their time variations, with a better phasing between CPP and ISBA/TRIP. Over the basin, the CPP and model anomalies globally corroborate in phase and amplitude.

Figure 9a show the monthly relative CPP flooded fraction averaged over the period 2002–2007. The monthly values have been divided by the maximum monthly value over 2002–2007 to determinate the main observed flooded areas. According to these observations, the main inundations occur between July and December in three principal regions: the inner delta in Mali, the Northern Nigeria and the Southern basin. Figure 9b shows the monthly spatial correlation between CPP and ISBA-TRIP when the model is forced by TRMM with floods and aquifers. Over the 3 principal inundated regions, the correlation is bigger than 0.4. This correlation does not change significantly according to the configuration of the model.

The impact of general flooded areas over the evaporation was investigated. For this, only the grid cells with a flooded fraction higher than 15 % for the configuration NOAQF were considered. These cells represent 11 % of the basin if the model is forced by TRMM and 7 % of the basin if the model is forced by RFEH rainfalls. Figure 10 presents the averaged relative difference of total monthly evaporation simulated on these cells with (red) and without (blue) floodplains when the model is forced by TRMM. The evaporation on flooded areas is generally higher with the flooding scheme than without floods, especially during the monsoon and post-monsoon periods (20 to more than 50 % higher). The same observations are done for the simulations forced by RFEH.

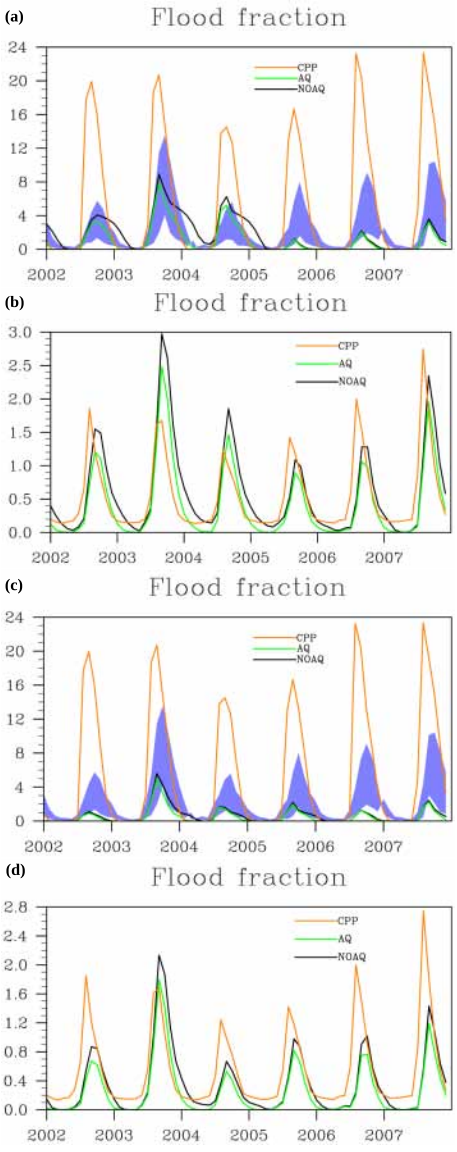

Fig. 7. (a) Time evolution of the mean monthly flooded fraction (in %) averaged over the inner delta region. The model is forced by TRMM-3B42. The blue range is the interval between the minimum and the maximum Modis classification (JFC) flooded fraction. **(b)** Time evolution of the mean monthly flooded fraction (in %) averaged over the basin. The model is forced by TRMM-3B42. **(c)** Time evolution of the mean monthly flooded fraction (in %) averaged over the inner delta region. The model is forced by RFEH. The blue range is the interval between the minimum and the maximum Modis classification (JFC) flooded fraction. **(d)** Time evolution of the mean monthly flooded fraction (in %) averaged over the basin. The model is forced by RFEH.

4.2.3 River height change

To complete the evaluation of surface water dynamics, the river height time changes are compared to estimates from the HYDROWEB hydrological database developed by the

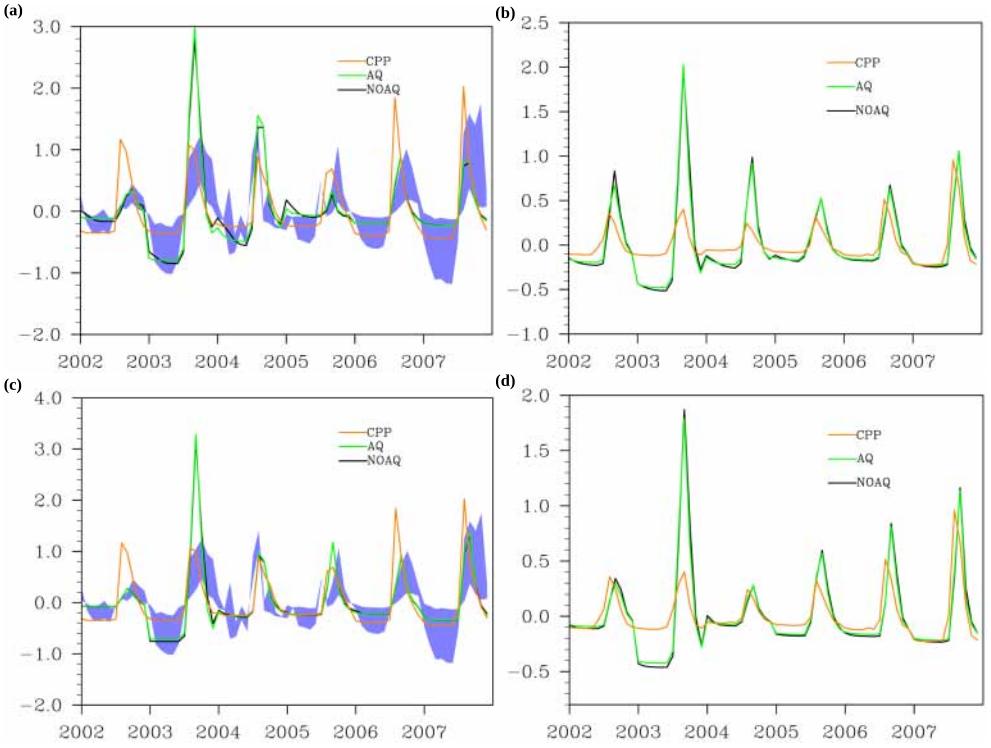

Fig. 8. (a) and **(c)** Time series of deseasonalized flood fraction anomalies (obtained by subtracting the 6-yr mean monthly value from individual months and then dividing by the standard deviation) over the delta. The blue range on the left figure delineates the maximum and minimum possible anomalies from Modis (JFC) products. The CPP product is orange. ISBA-TRIP without aquifers is in black and ISBA-TRIP with aquifers is in green. The TRMM-3B42 is used as forcing for **(a)** and RFEH is used for **(c)**. **(b)** and **(d)** Time series of deseasonalized flood fraction anomalies (obtained by subtracting the 6-yr mean monthly value from individual months and then dividing by the standard deviation) over the basin. The CPP product is orange. ISBA-TRIP without aquifers is in black and ISBA-TRIP with aquifers is in green. The TRMM-3B42 is used as forcing for **(b)** and RFEH is used for **(d)**.

LEGOS/GOHS (Calmant et al., 2008) which gives estimations of height changes at several points along the Niger river (Fig. 11). The seven locations used for comparison are noted in purple in Fig. 2. The bias error on the HYDROWEB water levels measures is estimated to be around 20 cm and the peaks of water height changes are within a range between 2 and 4 m. Since our interest is to be able to reproduce extreme events, this error is considered as reasonable for evaluating water height changes. The water level changes are represented in Fig. 11 for the four configurations when the model is forced by TRMM-3B42 rainfalls. The statistical scores are represented in Table 4 for the two rainfall datasets. The scores are generally improved by the presence of the flooding scheme. The addition of aquifers is more relevant when the model is forced by TRMM rainfall than RFEH. However, the scores are not greatly deteriorated by the presence of aquifers and considerably improved at the other sites. Without floodplains, the peaks of water height changes are overestimated. The model also overestimates the peaks of positive height changes which might be due to forcing anomalies (rain) or to model deficiencies. Indeed, the surface runoff stream function might be false in some areas and, if overestimated, results in an overestimation of water height variation during rain events. Also, uncertainties in the river bed slope can also result in an overestimation of the water height changes in the valleys. Moreover, Yamazaki et al. (2011) showed the limitation of the kinematic wave approach. Indeed, when kinematic wave equation is used for discharge calculation, the predictability of water surface elevation becomes bad in flat river basins with floodplains. However, no attempt is made to calibrate these parameters here, which would be a long and difficult process and which is not necessary for use in a GCM.

4.3 Total terrestrial water storage

For global applications, it is of interest to evaluate the time evolution of total water storage (TWS) in LSMs and the contribution of each component to the total storage. Figure 12 shows the comparison between 3 GRACE satellite products that estimate the total water storage (TWS) change globally at 1° resolution (the blue range in the lower panels represents the difference between the maximum and minimum monthly observation values) and the water storage change in all of the

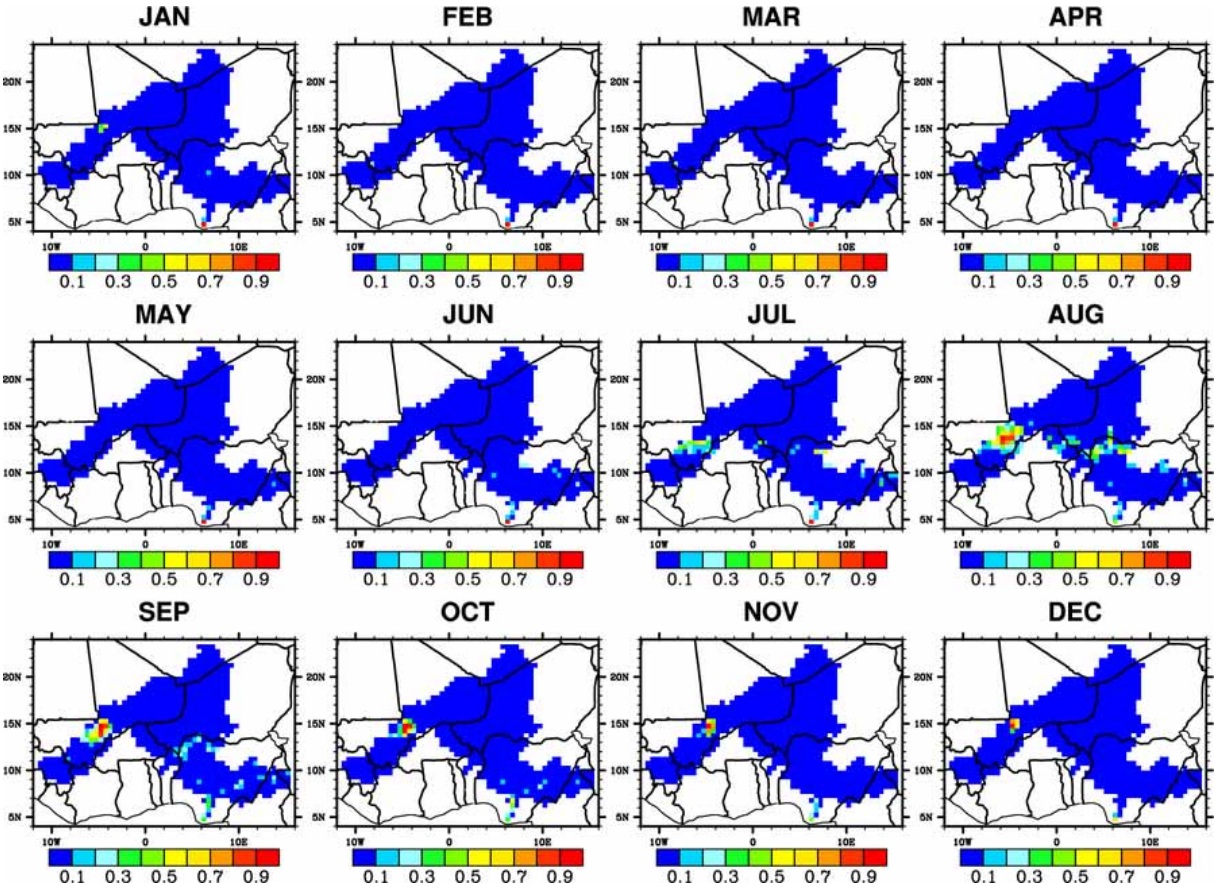

Fig. 9a. Spatial distribution of the normalized CPP flooded fraction averaged over 2002–2007 (the monthly value is devided by the maximum monthly value between 2002 and 2007).

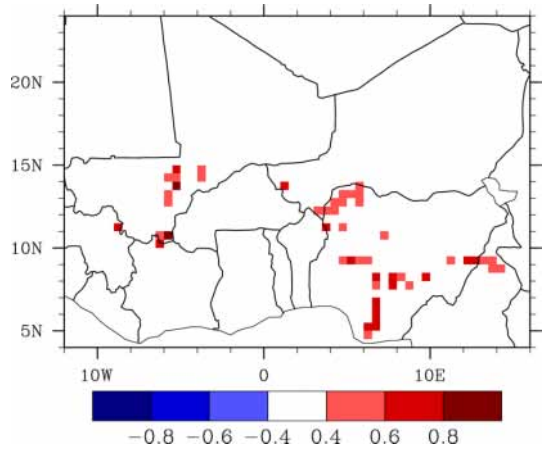

Fig. 9b. Spatial monthly correlation between ISBA-TRIP and CPP over 2002–2007.

Table 4. Correlations of the river height changes (from 2002 to 2007).

Corr. TRMM	1	2	3	4	5	6	7
NOAQNF	0.77	0.43	0.42	0.3	0.53	0.54	0.6
NOAQF	0.56	0.38	0.48	0.36	0.5	0.6	0.69
AQNF	**0.79**	0.38	0.41	0.3	0.54	0.53	0.61
AQF	0.7	**0.44**	**0.62**	**0.48**	**0.75**	**0.69**	**0.7**
Corr. RFEH							
NOAQNF	0.7	0.41	0.42	0.25	0.48	0.48	0.76
NOAQF	0.59	**0.43**	**0.65**	0.45	**0.69**	**0.76**	0.81
AQNF	**0.73**	0.39	0.41	0.24	0.49	0.48	0.79
AQF	0.68	0.4	0.63	**0.45**	0.67	0.74	**0.84**

reservoirs of the ISBA-TRIP model, averaged over the basin. The left panels represent the inter-annual variations (monthly means) and the right panels are the intra-annual variations (2003–2007 average for each month). The blue curve on the lower panels represents the mean water storage change of the Niger basin in all of the ISBA-TRIP reservoirs. The upper panels contain the water storage change in each reservoir (averaged over the basin) and the middle panels present the time evolution of the rain, drainage, runoff and evaporation over the basin. On the figure, only the results for the configuration AQ-F forced by TRMM are shown but Table 5 presents the correlations for each configuration. The comparison of

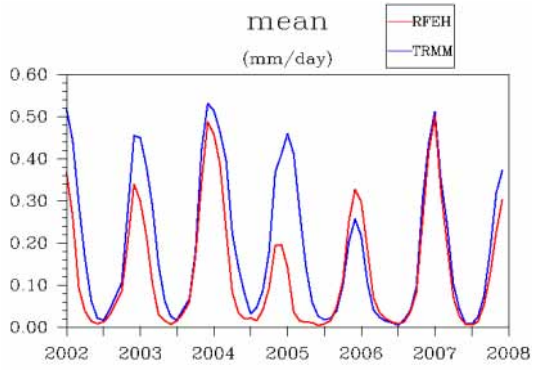

Fig. 10. Relative difference of evaporation between the two configurations NOAQ-NF and NOAQ-F. Only the cells with a monthly flooded fraction higher than 15 % over 2002–2007 are considered for the calculation.

ISBA-TRIP water storage change with the GRACE products over the Niger basin shows a very good correlation between the simulation and observations (more than 0.78) independantly of the configuration considered. The contributions of each reservoir to the total water storage change appear in the Table 6 for the configuration AQ-F. Although the uppermost soil layers (approximately 1 to a few meters) comprise most of the total water storage change over the basin (49 %), the contribution of the other reservoirs, such as the groundwater and the aquifer, are not negligible (17 % each). The contribution of flooded zones is less (4 %), but since their impact on evaporation is not negligible, they must be considered also. These results emphasize the need for considering all such reservoirs in LSMs in order to close the water budget. Generally, studies compare the GRACE water storage change to the water storage change in the hydrologic soil layers only, i.e. the first soil meters (green curve in the last panel). However, this approximation is likely less valid for regions with significant storage in flooded zones and deeper soil layers since the contribution of these two reservoirs to the total water storage are not necessarily negligible.

4.4 Rainfall comparison

A comparison of the rain datasets was done for every year. The averaged monthly ratio for every year (TRMM − RFEH)/(TRMM + RFEH), which represents the relative bias of one dataset to the other, has been calculated when the monthly sum (TRMM + RFEH) is bigger than 1mm/day. The most significant differencies are observed during the monsoon period and visible on Fig. 13 which presents the previous ratio for the months of July, August and September 2002–2007. The basin is delimitated by the black contour. Of note, significant differences are seen in the upper basin. From 2002 to 2004, the TRMM rainfall gives 20 to 80 % more rainfall than RFEH. This area is the main source

Table 5. Correlations of the model TWS with GRACE TWS (from 2002 to 2007).

Corr. TRMM	CSR	JPL	GFZ
NOAQ-NF	0.82	0.82	0.77
NOAQ-F	0.87	0.87	0.83
AQ-NF	0.84	0.83	0.79
AQ-F	0.87	0.86	0.82
Corr. RFEH			
NOAQ-NF	0.82	0.83	0.79
NOAQ-F	0.86	0.87	0.83
AQ-NF	0.83	0.84	0.8
AQ-F	0.86	0.86	0.83

Table 6. Contribution of the reservoirs for the configuration AQ-F forced by TRMM (%).

River	Soil	Floods	Aquifer	Groundwater
13	49	4	17	17

region for the river and this difference probably explains the fact that the discharge simulated when the model is forced by TRMM is generally bigger than the discharge when the model is forced by RFEH, in particular, when there is no flooding scheme (twice as large as than RFEH). Moreover, the discharge simulated using TRMM rainfall has a longer recession period, probably due to the fact that there is more water going from the floodplains to the river after the flooding season. Figure 13 also shows that in 2005, 2006 and 2007, the relative bias between the two datasets is no longer obvious. Looking at the discharge we can see that during these 2 yr, the two rainfall products produce a very similar discharge amplitude, which results in a big reduction of the discharge amplitude simulated by TRMM in comparison with previous years. One possible cause for the reduction in input rainfall is that the gauge analysis source was changed from the GPCC Monitoring analysis to the Climate Prediction Center (CPC) Climate Analysis and Monitoring System (CAMS) in May, 2005. This change was made to take advantage of the timeliness in CAMS, but in retrospect it introduced a discontinuity in the error characteristics of the gauge analysis (G. J. Huffman, personal communication, 2012).

4.5 Aquifer storage

Over the Niger basin, it was noticed that the discharge was still overestimated (Decharme et al., 2011). A possible identified cause was that these regions might overlie large aquifers that can be relatively uncoupled to the river. The available data concerning the aquifer storage are generally very localized, making the comparison with such a global scale model not relevant. Figure 14 shows the repartition of the aquifer recharge over the basin when the model is forced by

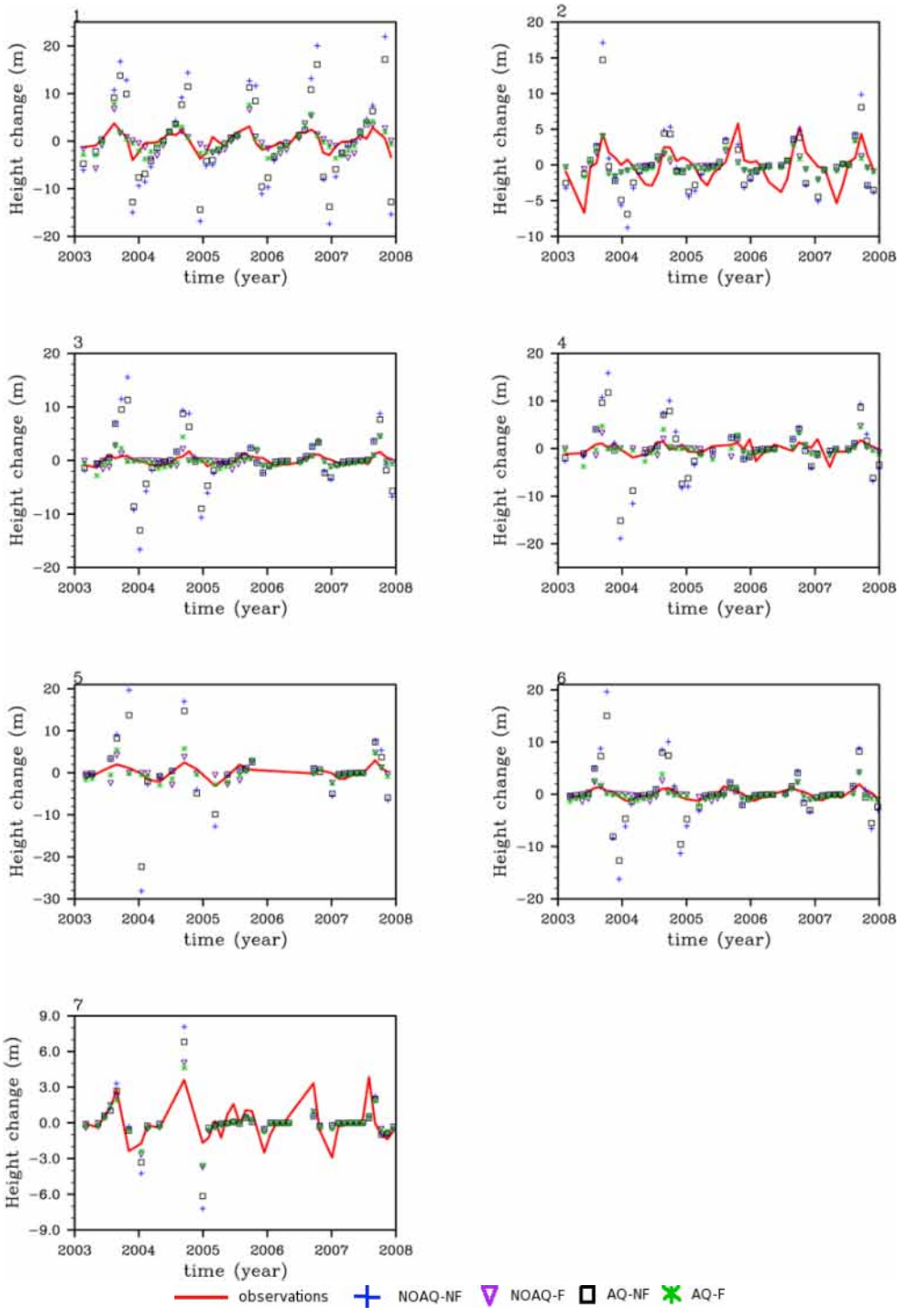

Fig. 11. Water level changes when the model is forced by TRMM.

RFEH. As expected, the aquifer recharge is very heterogeneous over the basin and follows rain patterns. There is also more aquifer recharge when the model is forced by TRMM than by RFEH. The aquifer reservoir is a relatively simple single-parameter linear reservoir and thus cannot represent high frequency fluctuations and distribution of the aquifer recharge. However, the analysis of total water storage have shown that its contribution to this total storage is not negligible and must be taken into account to reproduce the evolution of the water budget.

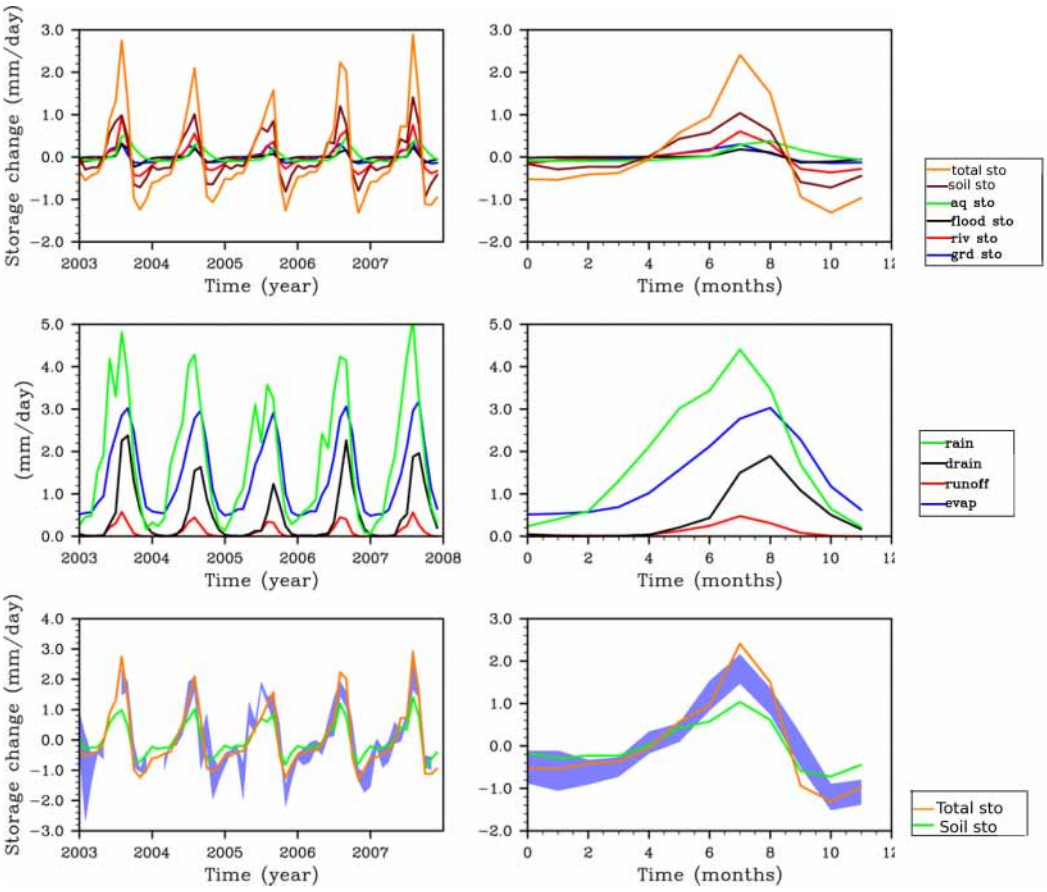

Fig. 12. Basin water storage change (mm day^{-1}) of each reservoir (top). Time evolution of rain, runoff, drainage and evaporation over the basin (middle). Basin water storage change (mm day^{-1}) in all reservoirs compared to GRACE datasets (down). The blue range is the difference between the maximum and the minimum GRACE products values. Left panels represent interannual variations (monthly averages) and right panels are the annual variations (each month is averaged over the whole 5 yr period).

4.6 Sensitivity tests

Sensitivity tests were performed to determine the input parameters which have the most significant impact on the simulations. For global simulations, it is preferable that the model is not sensitive to too many parameters since tuning is a long and fastidious process at the global scale and spatially distributed global scale observational data is currently rather limited. Generally, physiographic relationships or the derivation of secondary parameters are preferred. The sensitivity of the ISBA-TRIP model to several key input parameters was investigated in this study in order to test their importance for a single regional scale basin. The Table 7 presents the key input parameters and the variations applied. The RFEH rainfall datasets were used for this study but the sensitivity tests using TRMM-3B42 rainfall datasets lead to the same tendancies with lesser extent when forced by RFEH. Both rainfall datasets were used for this study. However, as sensitivity tests generally lead to the same tendancies according to the rainfall dataset used as forcing, the different figures show the results for only one rain forcing.

The impact of the river critical height, h_c, on the simulated discharge was examined first. The river width W is kept at the default value. Increasing the critical height by 20 % leads to 5 % less flooded fraction over the inner delta and in the south of the basin. The evaporation also decreases over the flooded zones by 4 to 12 % (relative bias). Conversely, when decreasing the river height by 20 %, the flooded fraction is 5 % more over the same areas and the evaporation is increased by 14 to 24 %.The water height changes are also influenced by the critical height modification. Over the 7 virtual sites, an increase of h_c globally increases the water height changes (+30 %), while a decrease of h_c decreases the water height changes (−16 %). This can be explained by the fact that a river with a small h_c will be flooded earlier and the water will spread more rapidly over the surrounding area, making the river water level less sensitive to rain events. In terms of inter-annual discharge, increasing or decreasing h_c, respectively, increases or decreases the amplitude of the discharge by 5 to 15 % (Fig. 15a and b). However, the annual variability of the discharge is not changed by a modification

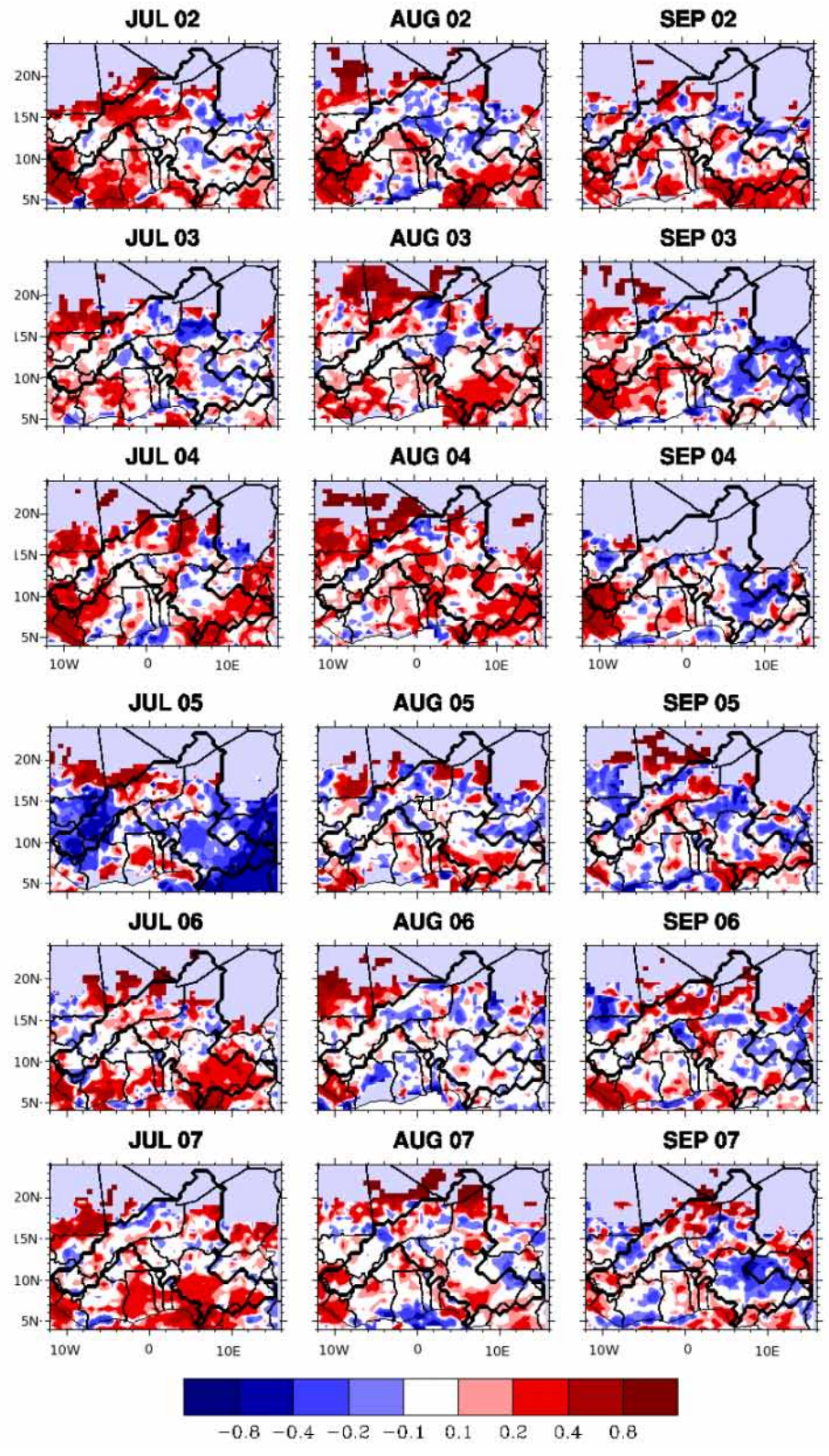

Fig. 13. Rainfall monthly averaged ratio (TRMM − RFEH)/(TRMM + RFEH). The ratio is calculated only when the sum TRMM + RFEH is bigger than 1 mm day^{-1}.

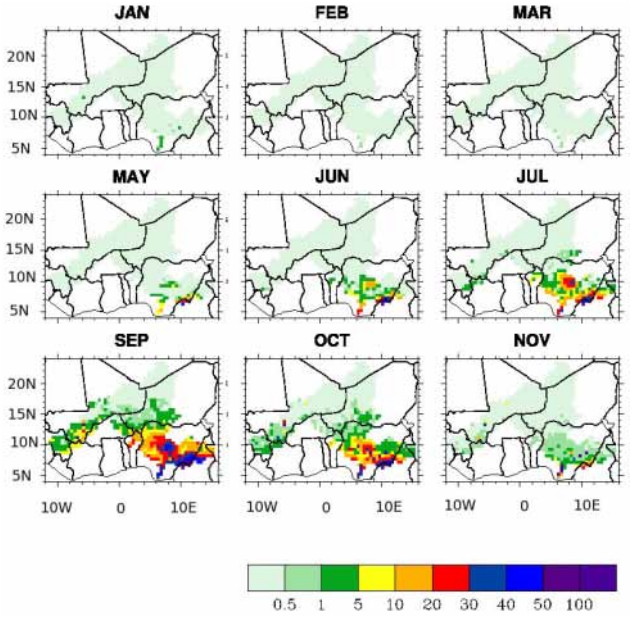

Fig. 14. Aquifer recharge distribution (mm yr^{-1})

of the critical height. In Niamey, Ansongo and Kandadji, the increase of h_c leads to better statistical scores, which might suggest that the model overestimates the flood extend in these areas. In contrast, in Malanville, the scores are better when reducing the critical height, which suggests an underestimation of flooding at this site. In Lokoja however, the scores are better for the standard simulation. The impact of the river width, W, was also investigated. The critical height is not changed. Increasing W increases the amplitude of the discharge by around 6 %, while decreasing arbitrary W by 20 % decreases the discharge by 9 % (Fig. 15c and d). The water height changes vary differently according to the site. For example, for location 1 (see Fig. 2 for locations), a 20 % reduction of the river width reduces the mean water height changes by 35 % over the studied period. However, for locations 2, 4, 5, 6 and 7, the mean water height changes increase by 15 % to 28 % and there is no change for location 3. Indeed, water height changes depend on the topography which is modified with river width variations. The evaporation over the flooded areas is reduced by 3 to 9 % when W increases and increased by 4 to 16 % when W decreases. There are no significant impacts of W and h_c on the total water storage change. Indeed, the storage of the different reservoirs and the amount of drainage are only slightly changed by the modification of these parameters.

The mean value of the Manning coefficient, n_{riv}, is around 0.075 and most of the pixels have values above 0.06 (91 out of 110). Since the Niger basin covers a large area, the soil properties are very heterogeneous all over the basin, making it necessary to use spatial distributions of soil parameters. Two new distributions of n_{riv} were created and used to

Table 7. ISBA/TRIP key input parameters and the variations applied for sensitivity tests.

Case 1	h_c	Spatially distributed constant in time	a. +20 % b. −20 %
Case 2	W	Spatially distributed constant in time	a. +20 % b. −20 %
Case 2	n_{riv}	Spatially distributed constant in time	a. +20 % b. −40 %
Case 4	τ	Constant in space and time	$\tau = 60; 90$
Case 5	τ_{aq}	Constant in space and time	$\tau_{aq} = 1; 16$
Case 7	α	Constant in space and time	$\alpha = \frac{1}{4}, \frac{1}{2}, \frac{3}{4}$

run the model: one distribution in which n_{riv} coefficient is arbitrary reduced by 40 % and the other one in which it is increased by 20 %. In order to keep a value included in a reasonable range (between 0.03 and 0.1), all the values out of this range after modification are set equal to the closest value in this range. Figure 16a shows the behaviour of the discharge for each distribution of n_{riv}. Increasing the Manning coefficient delays the response of the river to rain events. Indeed, small values of the coefficient speed the rise in water level and increase discharge amplitude. Also, the decrease of the discharge after the rainy season is faster when n_{riv} is smaller. We can also notice that when n_{riv} is bigger, the model is better able to dissociate the different rain events and two peaks of discharge appear. Flooded areas and evaporation are higher for large values of n_{riv} as the water flows more slowly in the river bed, generating smaller river height changes, and flooded areas empty to the river more slowly. The evaporation increases by 14 % over main evaporation areas when n_{riv} is 20 % higher and decreases by 18 % when it is 40 % smaller. Flooded areas are 15 % higher over the inner delta area when the Manning coefficient increases and 30 % smaller when it decreases. The increase of n_{riv} also delays the water height changes, while small values of n_{riv} decrease the peaks of river height changes. However, the impact of this coefficient on the water height change is more or less significant according to the observation sites, and for most of them this impact is not obvious. Finally, these modifications of n_{riv} have no significant impact on the total water storage change. Thus, the current distribution used in the model is the most reasonable according to the scores. The model is quite sensitive to Manning coefficient, which seems coherent. Since this coefficient is used for the calculation of the flow speed, it will impact the discharge, but also the creation of floods.

We also investigated the impact of increasing the groundwater reservoir's time delay factor on discharge, which extends the time of exchange between the groundwater reservoir and the river. Decharme et al. (2010) estimated that a time delay factor of the order of 30–60 days is generally

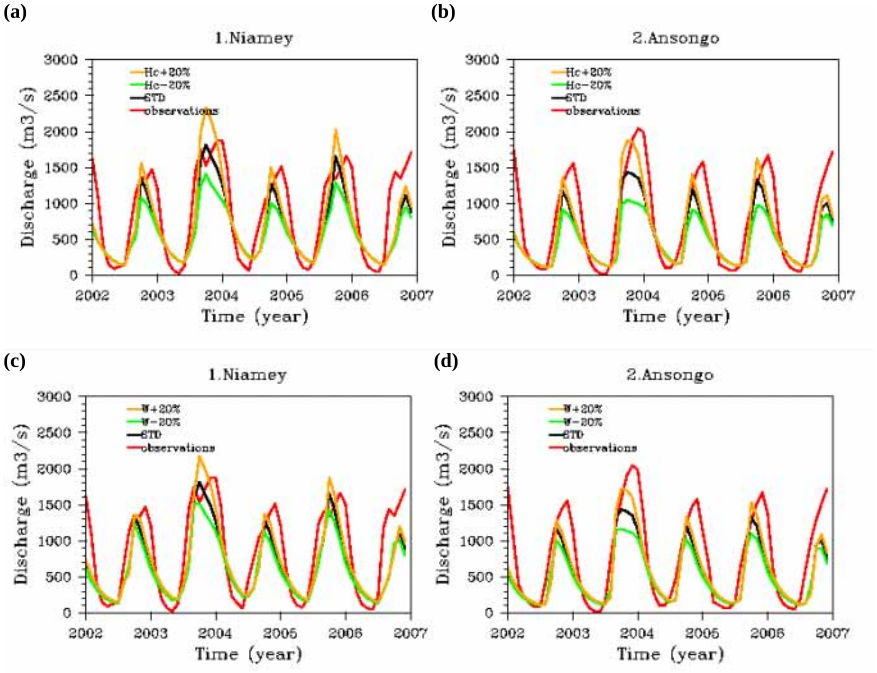

Fig. 15. Impact of modifications of the critical height h_c (**a** an **b**, up) and of the river width W (**c** and **d**, down) on the discharge (RFEH is used as forcing). The standard run stands for the simulation AQ-F with standard parameters (used for the simulations in previous sections).

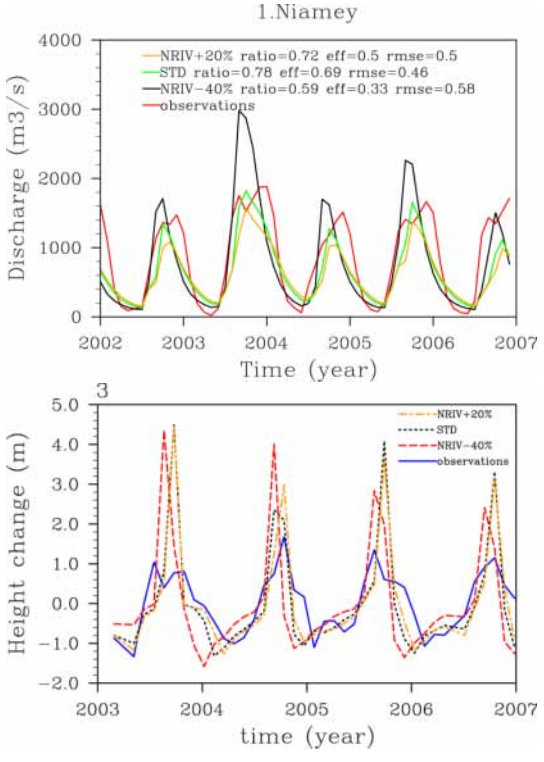

Fig. 16. Impact of the Manning coefficient on the river discharges and on the river height changes (RFEH is used as forcing). The standard run stands for the simulation AQ-F with standard parameters (used for the simulations in previous sections).

suitable for global simulations. The increase of τ impacts the discharge on the descending phase by deteriorating the recession law. The scores are not significantly changed by the increase of τ. The total water storage is not highly dependant on τ either (the mean variation represents about 5 % of the mean water storage change). However, previous results emphasized that this parameter is important since it increases the residence time of water storage in the basin and allows a more realistic simulation of the discharge.

Finally, we investigated the impact of parameter related to the aquifers. The reduction of the distribution factor α (which means an increase of the water going to the aquifer) decreases the discharge amplitude before the inner delta and accelerate the recession of the discharges after the inner delta (see Fig. 17). The scores are not significantly changed by the value of α when the model is forced by RFEH and experience only few changes when forced by TRMM-3B42. The aquifer reservoir time delay factor has also no impact on the discharge as aquifers are assumed to be too deep and too slow to impact directly the river discharge. Modifications of τ_{Aq} have a negligible impact on the total water storage of the basin (the mean variation represents less than 10 % of the mean water storage change). However, the simulation is done over a relatively short period (5 yr) over which the aquifer time delay factor might be less significant. Over longer periods of time, as for example for climatic studies, it is possible that water storage by aquifers and water discharge to the ocean has a significant impact on the water budget, and thus τ_{Aq} could be one key parameter contributing to the water balance.

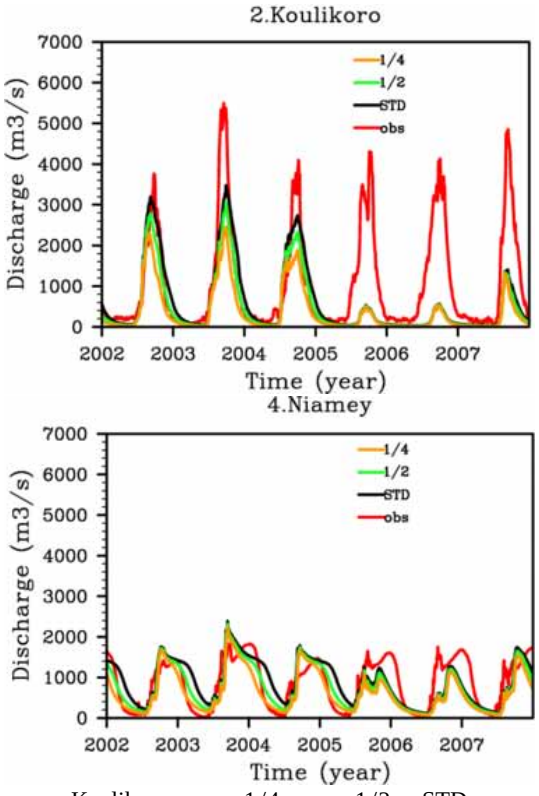

Koulikoro	$\alpha = 1/4$	$\alpha = 1/2$	STD
corr	0.72	0.7	0.66
rmse	1.11	1.04	0.54
eff	0.14	0.28	0.41
Niamey			
corr	0.77	0.77	0.68
rmse	0.53	0.48	0.46
0.44	0.54	0.59	

Fig. 17. Impact of aquifer distribution factor α on the discharge (TRMM is used as forcing). The standard run stands for the simulation AQ-F with standard parameters (used for the simulations in previous sections).

5 Discussion

The presented study investigated the impact of a linear flooding scheme and a simple aquifer storage on the simulation of the Niger basin. The flooding scheme decreases streamflow and increases evaporation over flooded areas. The impacts of floods on the water fluxes and storage terms are found to be coherent with other studies (Coe et al., 2008; Decharme et al., 2008, 2011; Dadson et al., 2010), thus we further emphasize the need for representing these processes in GCMs. Moreover, the observed data from the ABN have shown a clear change of behaviour of the discharge after the inner delta compared to the discharge before the delta (the discharge is almost divided by two), highlighting the role of the delta in the discharge reduction. This is coherent with the impact of the flooding scheme on the simulated discharge (divided by two after inclusion of floodplains in the model). However, it seems that in ISBA-TRIP, floods occur too early upstream of the delta, as suggested by the results in Ke Macina where the simulated discharge starts to be reduced while it is not the case in the observations. This might be due to poor values of the river parameters, such as river width in this particular region. The aquifer reservoir reduces the low flows and impacts the recession law, especially when the model is forced by TRMM. Moreover, its contribution to the total water budget is not negligible, and thus the consideration of aquifer processes is necessary to better simulate the evolution of the water cycle components. And indeed, several studies qualitatively suggest the presence of a deep water storage reservoir.

The results also suggest that the coupled land surface and river routing model provides a reasonable estimation of inland hydrological processes of the Niger basin when the flood scheme is activated and a deep aquifer is considered. Several diverse datasets have been used for model evaluation such as river discharge, spatial and temporal evolution of flooded areas and water height changes measured by satellite. These data provide basic constraints for estimating the sub-surface water storage and dynamics, but also the shallow soil water content and the groundwater storage, which are linearly related to the surface water. The comparison with GRACE total water storage dataset also show a good ability of the model to reproduce the evolution of total inland water.

Evapotranspiration is the remaining water budget component, but large scale observations are not available. The evaluation of this variable has been done within the context of several other studies. The ISBA surface temperature was evaluated using brightness temperatures from AMSR (de Rosnay et al., 2009), which is related to the surface energy budget and near surface soil moisture; and the monthly sensible heat fluxes aggregated from local scale observations to the ALMIP grid square were evaluated for a semi-arid region within the Niger basin (net radiation was imposed, thus monthly Bowen ratios can be estimated; Boone et al., 2009). Finally, regional scale water budget studies were performed over West Africa using ISBA evaporation estimates (Meynadier et al., 2010). All of the aforementioned studies imply that monthly scale evaporation estimates are reasonable.

Moreover, Mahe et al. (2009), estimated the water losses of the inner delta of the Niger river and their evolution from 1924 to 1996. They estimated the total evapotranspiration from the delta to be about 800 mm yr^{-1} over the period 1924–1996, varying between 400 mm yr^{-1} (1984) and 1300 mm yr^{-1} (1924). The total evapotranspiration calculated by ISBA over the period 2002–2006 is 662 mm yr^{-1}, which is contained in the range estimated by the previous study. They also related the water losses in the delta to the expansion of the floodplains, highlighting the importance of considering floods in a LSM.

However, some model deficiencies remain and can be due to different factors:

– A bias in the runoff and drainage calculated by the LSM. Further improvements could be obtained by calibrating the relevant parameters, but such a procedure is not relevant to GCM modelling.

– An over-simplified routing model. Indeed, global scale routing models are generally parametrized by geomorphologic relationships, which is not always realistic. Spatially distributed basin-specific parameters would undoubtably improve the simulations.

– Rain biases can also be the origine of model biases. In this study, we have seen that the generally accepted two best rainfall datasets over this region give significantly different results.

Sensitivity tests have shown that a good routing model is required to optimize the simulation errors. For example, Fig. 15 shows that while increasing h_c in Niamey, Kandadji and Ansongo would improve the simulation score, it would have the opposite effect in Malanville. Thus, improvements in remote sensing technologies should help to create maps of spatial and temporal evolution of inland waters (river width, flooded areas expansion, river height) and thus compensate the lack of in situ measurements. These data will then either be used as input data and replace geomorphologic relations used currently to describe these parameters, or they will be assimilated into the model to correct simulation errors.

In GCMs, the input parameters, such as the Manning coefficient, critical height, river width and depth, are defined by empirical relationships which might not give the best results for all modelled basins, since the main objective of such parameterizations is to give the best overall global results. However, for regional or basin scale studies, these relationships lead to non-negligible known errors which could be reduced using satellite data. Indeed, satellite data could be used to spatially distribute parameters by basin and then could contribute to the development of a global database describing the major river characteristics, at least the stream width and the river bankfull height. This is an important step if GCM climate scenario output is to be used for water resource management at the regional scale.

Input rainfall uncertainties can also be the cause of biases in the simulations, as shown in Sect. 4.1 where the model, forced by two different rain datasets, gives significantly different results. In this paper, only the TRMM-3B42 and TRMM-RFE2-hybrid rain dataset, RFEH, were used for the bulk of the validation. However, other rain datasets were used as input rainfall to run the ISBA-TRIP model, such as PERSIANN (Precipitation Estimation from Remotely Sensed Information using Artificial Neural Networks, http://chrs.web.uci.edu/persiann/) from the Center for hydrometeorology and remote sensing (CHRS) and CMORPH (CPC MORPHing technique, http://www.cpc.ncep.noaa.gov/products/janowiak/cmorph.shtml) from the United States National Oceanic and Atmospheric Administration (NOAA). The results of the simulations using both of these rainfall datasets showed a significant overestimation of the discharge (about 5 times higher than with the RFEH forcing for both CMORPH and PERSIANN forcing, and twice higher for the TRMM forcing) at all discharge observation sites, even with the representation of floods and aquifers. This is consistent with the work of Pierre et al. (2011) who showed that CMORPH dataset clearly overestimates precipitations over the Sahel. Improved spatially distributed remotely sensed datasets which are more precise for hydrological applications are thus needed.

6 Conclusions and perspectives

This study describes the evaluation of the ISBA-TRIP Continental Hydrologic System (CHS) over the Niger river basin, using a prognostic flooding scheme and a linear deep aquifer reservoir. The simulations are done at a 0.5° by 0.5° resolution over the 2002–2007 period. The flood scheme accounts explicitly for the precipitation interception by the floodplains, the direct evaporation from the free water surface and the possible re-infiltration into the soil. The deep aquifer reservoir has no feedback with the river locally and drains water to the river mouth over a comparatively long timescale. The model has been developed for use in climate model applications (coupled to the ARPEGE RCM and GCM at Météo France) where the representation of processes such as evaporation from the continental surface and freshwater fluxes to the ocean are fundamental to the global water budget. These applications especially aim at detecting strong anomalies in the future climate, and for this reason we focused on evaluating the ability of the model to reproduce inland waters anomalies. The model was run in four different configurations to evaluate the separated impacts of the flooding scheme and the aquifer reservoir on the modelisation of the Niger basin. Moreover, two different rainfall were used as forcing in order to take into account the impact of rain uncertainties on the simulations. The evaluation is done using a large variety of data, consisting of gauging measurements and satellite-derived products. This allows the spatially distributed evaluation of the separation of the water storage into its different components and it gives a first estimate of aquifer dynamics over the basin.

Considering the relative simplicity of the routing channel, the model provides a good estimation of the surface water dynamics: the spatio-temporal variability of the flooded areas, the river discharge and the river water height changes. The flooding scheme leads to an increase of evaporation and reduction of discharge after the inner delta area, testifying for the need to incorporate flood representations into land surface models (LSMs). The behaviour of the observed discharge also suggest an impact of the inner delta, known as an important flooded area, on the discharge. The aquifer reservoir impacts the representation of both low flows and the

recession law during the dry season. Note that recently an option to include a detailed representation of aquifers has been introduced into the ISBA-TRIP CHS (Vergnes et al., 2012). However, the quality of the input and observational data required to evaluate the scheme is currently lacking over the Niger basin. For this reason we have opted for a more simple linear reservoir approach in this study (consistent with the other TRIP reservoirs). However, the possible link between river height and aquifer storage will be explored using remotely sensed data in future work. The comparisons with GRACE total water storage change (GFZ, CSR and JPL) were used to evaluate the ability of the model to reproduce the evolution of the total inland water, and good overall agreement of total water stored with GRACE was found. Finally, the use of two different rainfall datasets as forcing has shown the sensitivity of the model to rain uncertainties.

Despite the fact that the main features of the river dynamics and water budget terms are represented reasonably well by this relatively simple system, some simulation deficiencies remain. For example, the model has a difficulty in terms of reproducing the discharge during the low flow period or the two annual peaks of discharge (only one peak is reproduced by the model). These deficiencies might be due to precipitation uncertainties or LSM errors (in terms of subgrid runoff, evaporation and soil water transfer physics, input LSM physiographic parameters such as vegetation indicies, soil texture and depth, etc.): but the focus in this study is mainly on river, floodplain and aquifer dynamics. Precipitation uncertainties were briefly touched upon by using different input forcings, but few currently available rainfall products are good enough to be useful for hydrological modelling studies over this region (notably owing to large biases). Regarding the RRM errors, Decharme et al. (2011) have discussed the questionable aspects of the flooding scheme such as the empirical computation of the river width, the choice of the river bankfull height, the simplified geometry of river stream and flood reservoirs, or the use of the Manning's formula for computing the mass transfer between them. Moreover, sensitivity tests have shown the non-negligible impact of some of the parameter values on simulations. However, the model has been developed for global climate applications at low resolutions and must be as robust as possible to be applicable at global scale, and therefore has a limited number of tunable parameters. However, upcoming advances in remote sensing technologies should permit an optimization of the spatially distributed parameters of the model. In fact, forcing uncertainties, especially rain uncertainties, represent a limitation for model tuning at this scale. Moreover, they can compensate the non-representation of lakes and large ponds.

A global database describing the basin characteristics such as the river width and the bankfull height would be of great interest for improving the model simulations. This likely depends heavily on advances in remote sensing technologies, which should help to get maps of spatial and temporal evolution of inland waters (river width, flooded areas expansion, river height, etc.) and thus compensate for the lack of in situ measurements at the global scale. The joint CNES-NASA satellite project SWOT will provide water heights and extent at land surface with an unprecedented 50–100 m resolution and precision (centimetric accuracy when averaged over areas of 1 km; Durand et al., 2010). These data will then either be used as input data and replace geomorphologic relations used currently to describe surface parameters, or they will be assimilated into the model to correct model errors. Indeed, a small number of recent studies have begun to quantify the benefits of such a mission for land surface hydrology. For this purpose, synthetic water elevation data were created using the JPL Instrument Simulator (Rodriguez and Moller, 2004) and assimilated into CHS systems (Durand et al., 2008; Biancamaria et al., 2010). In all of these studies, the assimilation of synthetically generated SWOT measurements helped to reduce model errors and improved river discharge simulation. Other studies have used SWOT simulated data as inputs in algorithms to obtain estimates of river depth and discharge (Andreadis et al., 2007; Durand et al., 2010; Biancamaria et al., 2010, 2011). These preliminary results are promising and show the current need for such a mission, and the potential for improving the representation of hydrological processes in current models. Consequently, the next step of this work will consist of integrating synthetic SWOT data into a suitable assimilation system to determine their impact on the simulated discharge using the ISBA-TRIP CHS described herein.

Appendix A

The TRIP river discharge and groundwater outflow

The river discharge simulated by TRIP (Eq. 1) is computed using a streamflow variable velocity, v ($\mathrm{m\,s^{-1}}$), and via the Manning's formula:

$$Q_{\mathrm{out}}^{S} = \frac{v}{L} S \quad \text{with} \quad v = \frac{\kappa}{n_{\mathrm{riv}}} R^{2/3} s^{1/2}, \tag{A1}$$

where L (m) is the river length that takes into account a meandering ratio of 1.4 as proposed by Oki and Sud (1998), s ($\mathrm{m\,m^{-1}}$) is the downstream river height loss per unit length approximated as the river bed slope, R (m) the hydraulic radius, κ ($\mathrm{m^{-3}\,s^{-1}}$) a constant equal to 1, and n_{riv} the dimensionless Manning friction factor which varies from the upstream part to the mouth of each basin. The river bed slope is indeed a critical parameter to compute velocity via the Manning formula. The STN-30p Digital Elevation Model (DEM) provided at 0.5 °C by 0.5 °C resolution by the ISLSCP2 database (http://www.gewex.org/islscpdata.htm) has been used. The STN-30p DEM was heavily edited to represent the actual elevation along the river network on a global scale, based on the aggregated HYDRO1 K DEM at 1 km resolution. Further adjustments were made to eliminate some of the unrealistic rapid slope changes in the STN-30p

DEM along the global river network. Yamazaki et al. (2009), included a realistic sub-grid-scale topography for a more reasonnable representation of the river height loss. This inclusion could be considered as a possible improvement of the representation of the river bed slope in the TRIP model. The hydraulic radius is related to the stream water depth, h_s (m), calculated from the stream water mass, S (kg), assuming a rectangular river cross-section (Arora and Boer, 1999):

$$R = \frac{W\, h_s}{W + 2\, h_s} \quad \text{where} \quad h_s = \frac{S}{L\, W \rho_W}, \tag{A2}$$

where ρ_W (kg m^{-3}) is the water density, and W (m) the bankfull river width.

The TRIP groundwater outflow (Eq. 1) is computed using the following simple linear relationship proposed by Arora and Boer (1999):

$$Q_{out}^G = \frac{G}{\tau} \tag{A3}$$

where τ (s) is an uniform and constant time delay factor of the groundwater reservoir which is fixed to 30 days. This groundwater reservoir does not represent the groundwater dynamics but only delays the groundwater flow contribution to the surface river reservoir within a particular grid cell: the deep drainage is fed into the surface reservoir with a time delay factor of τ. More details can be found in Decharme et al. (2010).

Appendix B

The ISBA-TRIP flood model

As shown in Fig. 1, a simplified rectangular geometry is assumed in TRIP to represent the cross section between the floodplain and the river reservoirs in each grid cell. River flooding arises when the water height of the stream reservoir is higher than the critical bankfull height, h_c (m), and the flood outflow and inflow from this reservoir (Eq. 1) are given by:

$$\begin{cases} Q_{in}^F = \frac{v_{in}}{W + W_f}\, M_f \\ Q_{out}^F = \frac{v_{out}}{W + W_f} \min\,(M_f,\ F)\,, \end{cases} \tag{B1}$$

where W_f (m) is the floodplain width, and M_f (kg) the potential inflow (positive M_f) or outflow (negative M_f). This outflow assumes an equilibrium state between the stream and the floodplain water depth:

$$M_f = \rho_W\, L_f\, W\, (h_s - h_c - h_f)\,, \tag{B2}$$

where L_f (m) and h_f (m) are the length along the river and the depth of the floodplains, h_s (m) the water height of the stream reservoir, and h_c (m) the critical bankfull river height. $W + W_f$ represents the distance covered by M_f from the stream to the floodplains or conversely. v_{in} and v_{out} (m s^{-1}) are the flood inflow and outflow velocities, respectively, computed using the Manning's formula:

$$v_{in,out} = \frac{s_{in,out}^{1/2}}{n_f}\, R_{in,out}^{2/3}\,, \tag{B3}$$

where n_f is the Manning roughness coefficient for the floodplains that varies according to the vegetation type (Decharme et al., 2011), while $s_{in,out}$ (m m^{-1}) and $R_{in,out}$ (m) are the inflow (or outflow) slope and hydraulic radius, respectively, at the interface between the floodplain and the river stream.

The flood inflow and outflow velocities computed using the Manning's formula require the hydrological slope between the floodplain and the river stream:

$$\begin{cases} s_{in} = \frac{\max(0, h_s - h_c - h_f)}{(W + W_f)/2} \\ s_{out} = \frac{\max(0, h_f + h_c - h_s)}{(W + W_f)/2}. \end{cases} \tag{B4}$$

They also require the hydraulic radius assumed rectangular and calculated as follows:

$$\begin{cases} R_{in} = \frac{L_f \times \max(0, h_s - h_c)}{L_f + 2 \times \max(0, h_s - h_c)} \\ R_{out} = \frac{L_f h_f}{L_f + 2h_f}, \end{cases} \tag{B5}$$

where W_f (m), L_f (m) and h_f (m) are the width, the length and the depth (respectively) of the floodplains, h_s (m) the water height of the stream reservoir, h_c (m) the critical height of the river bed, and W (m) the stream river width. The hf is calculated in each grid-cell with the help of the actual distribution of the local height, h_i (m), determined at a 1 km by 1 km resolution. The assumption is that each pixel, i, represents a subbasin into a given grid-cell that can be potentially flooded. Each subbasin has a triangular form and is associated with a fraction, f_i, of the grid cell area, A. The h_i is computed using the local slope, τ_i (°) and flow direction data given by the HYDRO1 K dataset (Verdin and Greenlee, 1996):

$$h_i = l\sqrt{\alpha_i}\tan(\frac{\sigma_i \pi}{180}), \tag{B6}$$

where l (m) is the characteristic length of one pixel equal to 1000 m, and α_i is equal to 1 if the local flow direction is north, south, east, or west, and to 2 elsewhere. Therefore, for each hi a potential mass of flood, $V(h_i)$ (kg), can be simply calculated using a discrete equation:

$$V(h_i) = \rho_w \sum_0^i V_i \text{ where } V_i = \frac{A f_i h_i}{2}. \tag{B7}$$

The sub-grid distributions of the flooded fraction and the flood depth allow to determine f_{flood}, and h_f at each time step and in each grid-cell via the comparison between the water mass into the floodplain reservoir, F, computed by TRIP

(Eq. 4) and the sub-grid distribution of this potential mass $V(h_i)$:

$$F = V(h_i) \Rightarrow \left| \begin{array}{l} f_{\text{flood}} = \sum_{0}^{i} f_i \\ h_{\text{f}} = h_i. \end{array} \right. \quad \text{(B8)}$$

When f_{flood} is known within the grid cell, W_{f} and L_{f} are simply calculated as follow:

$$\left| \begin{array}{l} L_{\text{f}} = \max(0.001, r\sqrt{f_{\text{flood}A}}) \\ W_{\text{f}} = \frac{A f_{\text{flood}}}{L_{\text{f}}}, \end{array} \right. \quad \text{(B9)}$$

where r is the meandering ratio fixed to 1.4 as recommended by Oki and Sud (1998).

Finally, the precipitation interception by the floodplains, P_{f}, the re-infiltration, I_{f} , and the direct free water surface evaporation, E_{f}, (Eq. 1) are estimated by ISBA. I_{f} occurs if the flooded fraction, f_{flood}, calculated according to the sub-grid topography (Decharme et al., 2011), is superior to the soil saturated fraction, f_{sat}, and depends on the soil maximum infiltration capacity. In other words, the floodplains cannot infiltrate the fraction of the grid-cell for which the soil is saturated. To a first approximation, it allows to simply represent the fact that the actual floodplains evolve according to the presence of shallow aquifer and water table depth variations. More details can be found in Decharme et al. (2011).

Appendix C

List of acronyms.

AGCM	Atmospheric General Circulation Models
ALMIP	AMMA Land Surface Model Intercomparison
AMMA	African Monsoon Multidisciplinary Analysis
CHS	Continental Hydrologic System
GRACE	Gravity Recovery and Climated Experiment
HYCOS	Hydrologic Observation System
ISBA	Interactions Sol-Biosphère-Atmosphère
Land-SAF	Land Satellite Application Facility
LSM	Land Surface Model
MODIS	Moderate Resolution Imaging Spectroradiometer
NDVI	Normalized Difference Vegetation Index
RFE2	Rainfall Estimates version 2.0
RFEH	RFE-Hybrid
RRM	River Routing Model
SWOT	Surface Water Ocean Topography
TRIP	Total Runoff Integrating Pathways
TRMM	Tropical Rainfall Measuring Mission

Acknowledgements. This work is supported by the African Monsoon Multidisciplinary Analysis (AMMA) project and the Surface Water Ocean Topography (SWOT) satellite mission project of the "Centre National d'Etudes Spatiales" (CNES). The diverse studies presented in this paper would not have been possible without the valuable contribution of the "Autorité du Bassin du Niger" (ABN) and Catherine Prigent from the "Laboratoire d'Etudes du Rayonnement et de la Matière en Astrophysique".

Edited by: Y. Fan

The publication of this article is financed by CNRS-INSU.

References

Ali, A. and Lebel, T.: The Sahelian standardized rainfall index revisited, Int. J. Climatol., 29, 1705–1714, 2009.

Alkama, M. R., Kageyama, M., Ramstein, G., Marti, O., Ribstein, P., and Swingedouw, D.: Impact of a realistic river routing in coupled ocean-atmosphere simulations of the Last Glacial Maximum climate, Clim. Dynam., 30, 855–869, 2008.

Alkama, R., Decharme, B., Douville, H., Becker, M., Cazenave, A., Sheffield, J., Voldoire, A., Tyteca, S., and Le Moigne, P.: Global evaluation of the ISBA/TRIP continental hydrological system, Part 1: Comparison to GRACE terrestrial water storage estimates and in situ river discharges, J. Hydrometeorol., 11, 583–600, 2010.

Alsdorf, D. E. and Lettenmaier, D. P.: Tracking fresh water from space, Science, 301, 5639, doi:10.1126/science.1089802, 2003.

Alsdorf, D. E., Rodriguez, E., and Lettenmaier, D. P.: Measuring surface water from 593 space, Rev. Geophys., 45, RG2002, doi:10.1029/2006RG000197, 2007.

Amogu, O., Descroix, L., Yero, K. S., Le Breton, E., Mamadou, I., Ali, A., Vischel, T., Bader, J., Moussa, I. B., Gautier, E., Boubkraoui, S., and Belleudy, P.: Increasing River Flows in the Sahel?, Water, 2, 170–199, 2010.

Andersen, I., Dione, O., Jarosewich-Holder, M., and Olivry, J. C.: The Niger river basin: A vision for sustainable management, World Bank Publications, 2005.

Andreadis, K. M., Clark, E. A., Lettenmaier, D. P., and Alsdorf, D. E.: Prospects for river discharge and depth estimation through assimilation of swath-altimetry into a raster-based hydrodynamics model, Geophys. Res. Lett., 34, L10403, doi:10.1029/2007GL029721, 2007.

Arora, V. K. and Boer, G. J.: A variable velocity flow routing algorithm for GCMs, J. Geophys. Res., 104, 30965–30979, doi:10.1029/1999JD900905, 1999.

Beven, K. J. and Kirkby, M. J.: A physically-based variable contributing area model of basin hydrology, Hydrol. Sci. Bull., 24, 43–69, 1979.

Biancamaria, S., Andreadis, K. M., Durand, M., Clark, E. A., Rodriguez, E., Mognard, N. M., Alsdorf, D. E., Lettenmaier, D. P., and Oudin, Y.: Preliminary Characterization of SWOT Hydrology Error Budget and Global Capabilities, IEEE J. Sel. Top. Appl., 3, 6–19, doi:10.1109/JSTARS.2009.2034614, 2010.

Biancamaria, S., Durand, M., Andreadis, K. M., Bates, P. D., Boone, A., Mognard, N. M., Rodriguez, E., Alsdorf, D. E., Lettenmaier, D. P., and Clark, E. A.: Assimilation of virtual wide swath altimetry to improve Arctic river modeling, Remote Sens. Environ., 115, 373–381, 2011.

Bonan, G. B.: Sensitivity of a GCM to inclusion of inland water surfaces, J. Climate, 8, 2691–2704, doi:10.1175/1520-0442(1995)008¡2691:SOAGST¿2.0.CO;2, 1995.

Boone, A., Calvet, J.-C., and Noilhan, J.: Inclusion of a Third Soil Layer in a Land-Surface Scheme using the Force-Restore method, J. Appl. Meteorol., 38, 1611–1630, 1999.

Boone, A., de Rosnay, P., Basalmo, G., Beljaars, A., Chopin, F., Decharme, B., Delire, C., Ducharne, A., Gascoin, S., Grippa, M., Guichard, F., Gusev, Y., Harris, P., Jarlan, L., Kergoat, L., Mougin, E., Nasonova, O., Norgaard, A., Orgeval, T., Ottlé, C., Poccard-Leclercq, I., Polcher, J., Sandholt, I., Saux-Picart, S., Taylor, C., and Xue, Y.: The AMMA Land Surface Model Intercomparison Project, B. Am. Meteorol. Soc., 90, 1865–1880, doi:10.1175/2009BAMS2786.1, 2009.

Bousquet, P., Ciais, P., Miller, J. B., Dlugokencky, E. J., Hauglustaine, D. A., Prigent, C., Van der Werf, G. R., Peylin, P., Brunke, E. G., Carouge, C., Langenfelds, R. L., Lathiere, J., Papa, F., Ramonet, M., Schmidt, M., Steele, L. P., Tyler, S. C., and White, J.: Contribution of anthropogenic and natural sources to atmospheric methane variability, Nature, 443, 439–443, doi:10.1038/nature05132, 2006.

Calmant, S., Seyler, F., and Cretaux, J. F.: Monitoring Continental Surface Waters by Satellite Altimetry, Surv. Geophys., 29, 247–269, 2008.

Coe, M. T.: A linked global model of terrestrial processes: Simulation of modern rivers, 781 lakes and wetlands, J. Geophys. Res., 103, 8885–8899, 1998.

Coe, M. T.: Modeling terrestrial hydrological systems at the continental scale: Testing the accuracy of an atmospheric GCM, J. Climate, 13, 686–704, doi:10.1175/1520-0442(2000)013<0686:MTHSAT>2.0.CO;2, 2000.

Coe, M. T. and Birkett, C. M.: Calculation of river discharge and prediction of lake Height from satellite radar altimetry: example of the lake Chad basin, Water Resour. Res., 40, W10205, doi:10.1029/2003WR002543, 2004.

Coe, M. T., Costa, M. H., and Howard, E. A.: Simulating the surface waters of the Amazon River basin: impact of new river geomorphic and flow parameterizations, Hydrol. Process., 22, 2542–2553, doi:10.1002/hyp.6850, 2008.

Cogley, J. G.: The albedo of water as a function of latitude, Mon. Weather Rev., 107, 775–781, doi:10.1175/1520-0493(1979)107¡0775:TAOWAA¿2.0.CO;2, 1979.

Costa, M. H. and Foley, J. A.: Water balance of the Amazon Basin: Dependence on vegetation cover and canopy conductance, J. Geophys. Res., 102, 973–989, doi:10.1029/97JD01865, 1997.

Dadson, S. J., Ashpole, I., Harris, P., Davies, H. N., Clark, D. B., Blyth, E., and Taylor, C. M.: Wetland inundation dynamics in a model of land surface climate: Evaluation in the Niger inland delta region, J. Geophys. Res., 115, D23114, doi:10.1029/2010JD014474, 2010.

Dai, T. and Labadie, J. W.: River basin network model for integrated water quantity/quality management, J. Water Resour. Pl.-ASCE, 127, 295–305, 2001.

de Rosnay, P., Drusch, M., Boone, A., Balsamo, G., Decharme, B., Harris, P., Kerr, Y., Pellarin, T., Polcher, J., and Wigneron, J.-P.: AMMA Land Surface Model Intercomparison Experiment coupled to the Community Microwave Emission Model: ALMIP-MEM, J. Geophys. Res., 114, D05108, doi:10.1029/2008JD010724, 2009.

Decharme, B.: Influence of runoff parameterization on continental hydrology: Comparison between the Noah and the ISBA land surface models, J. Geophys. Res., 112, D19108, doi:10.1029/2007JD008463, 2007.

Decharme, B. and Douville, H.: Introduction of a sub-grid hydrology in the ISBA land surface model, Clim. Dynam., 26, 65–78, 2006.

Decharme, B., Douville, H., Boone, A., Habets, F., and Noilhan, J.: Impact of an exponential profile of saturated hydraulic conductivity within the ISBA LSM: simulations over the Rhône basin, J. Hydrometeorol., 7, 61–80, 2006.

Decharme, B., Douville, H., Prigent, C., Papa, F., and Aires, F.: A new river flooding scheme for global climate applications: Offline evaluation over South America, J. Geophys. Res., 113, D11110, doi:10.1029/2007JD009376, 2008.

Decharme, B., Alkama, R., Douville, H., Becker, M., and Cazenave, A.: Global evaluation of the ISBA-TRIP continental hydrological system, Part II: Uncertainties in river routing simulation related to flow velocity and groundwater storage, J. Hydrometeorol., 11, 601–617, 2010.

Decharme, B., Alkama, R., Papa, F., Faroux, S., Douville, H., and Prigent, C.: Global off-line evaluation of the ISBA-TRIP flood model, Clim. Dynam., 38, 1389–1412, doi:10.1007/s00382-011-1054-9, in press, 2011.

Dirmeyer, P. A.: Using a global soil wetness dataset to improve seasonal climate simulation, J. Climate, 13, 2900–2922, 2000.

Dirmeyer, P. A.: Climate drift in a coupled landatmosphere model. J. Hydrometeorol., 2, 89–100, 2001.

Dirmeyer, P. A., Gao, X., Zhao, M., Guo, Z., Oki, T., and Hanasaki, N.: GSWP-2: Multimodel analysis and implications for our perception of the land surface, B. Am. Meteorol. Soc., 87, 1381–1397, 2006.

Douville, H.: Assessing the influence of soil moisture on seasonal climate variability with AGCMs, J. Hydrometeor., 4, 1044–1066, 2003.

Douville, H.: Relevance of soil moisture for seasonal atmospheric predictions: Is it an initial value problem?, Clim. Dynam., 22, 429–446, 2004.

Douville, H., Planton, S., Royer, J. F., Stephenson, D. B, Tyteca, S., Kergoat, L., Lafont, S., and Betts, R. A.: Importance of vegetation feedbacks in doubled-CO_2 climate experiments, J. Geophys. Res., 105, 14841–14861, 2000.

Dunn, C. E., Bertiger, W., Bar-Sever, Y., Desai, S., Haines, B., Kuang, D., Franklin, G., Harris, I., Kruizinga, G., Meehan, T., Nandi, S., Nguyen, D., Rogstad, T., Thomas, J. B., Tien, J., Romans, L., Watkins, M., Wu, S.-C., Bettadpur, S., and Kim, J.: Instrument of GRACE:GPS augments gravity measurements, application challenge, GPS World, 2003.

Durand, M., Andreadis, K. M., Alsdorf, D. E., Lettenmaier, D. P., Moller, D., and Wilson, M.: Estimation of bathymetric depth and slope from data assimilation of swath altimetry into a hydrodynamic model, Geophys. Res. Lett., 35, L20401, doi:10.1029/2008GL034150, 2008.

Durand, M., Rodriguez, E., Alsdorf, D. E., and Trigg, M.: Estimating River Depth From Remote Sensing Swath Interferometry Measurements of River Height, Slope, and Width, IEEE J. Sel. Top. Appl., 3, 20–31, doi:10.1109/JSTARS.2009.2033453, 2010.

Enjolras, V. M. and Rodriguez, E.: Using altimetry waveform data and ancillary information from SRTM, Landsat, and MODIS to retrieve river characteristics, IEEE T. Geosci. Remote., 47, 1869–1881, 2009.

Fontes, J.-C., Andrews, J. N., Edmunds, W. M., Guerre, A., and Travi, Y.: Paleorecharge by the Niger River (Mali) deduced from groundwater geochemistry, Water Resour. Res., 27, 199–214, 1991.

Gedney, N., Cox, P. M., Douville, H., Polcher, J., and Valdes, J. P.: Characterizing GCM land surface schemes to understand their responses to climate change, J. Climate, 13, 3066–3079, 2000.

Geiger, B., Meurey, C., Lajas, D., Franchistéguy, L., Carrer, D., and Roujean, J-.L.: Near real-time provision of downwelling shortwave radiation estimates derived from satellite observations, Meteorol. Appl., 15, 411–420, 2008.

Getirana, A. C. V., Bonnet, M.-P., Rotunno, O. C., Collischonn, W., Guyot, J. L., Seyler, F., and Mansur, W. J.: Hydrological modelling and water balance of the Negro River basin: evaluation based on in situ and spatial altimetry data, Hydrol. Process., 24, 3219–3236, 2010.

Grippa, M., Mognard, N. M., Letoan, T., and Josberger, E. G.: Siberia snow depth climatology from SSM/I data using a combined dynamic and static algorithm, Remote Sens. Environ., 93, 30–41, 2004.

Grippa, M., Kergoat, L., Frappart, F., Araud, Q., Boone, A., de Rosnay, P., Lemoine, J.-M., Gascoin, S., Balsamo, G., Ottlé, C., Decharme, B., Saux-Picart, S., and Ramillien, G.: Land water storage variability over West Africa estimated by GRACE and land surface models, Water Resour. Res., Water Resour. Res., 47, W05549, doi:10.1029/2009WR008856, 2011.

Habets, F., Boone, A., Champeaux, J.-L., Etchevers, P., Franchistéguy, L., Leblois, E., Ledoux, E., Le Moigne, P., Martin, E., Morel, S., Noilhan, J., Quintana Seguì, P., Rousset-Regimbeau, F., and Viennot, P.: The SAFRAN-ISBA-MODCOU hydrometeorological model applied over France, J. Geophys. Res., 113, D06113, doi:10.1029/2007JD008548, 2008.

Haines, B., Dunn, C., Kim, J., Bar-Sever, Y., Desai, S., Kuang, D., Franklin, G., Harris, I., Kruizinga, G., Meehan, T., Nandi, S., Nguyen, D., Rogstad, T., Thomas, J. B., Tien, J., Romans, L., Watkins, M., Wu, S. C., Bettadpur, S., and Bertiger, W.: Instrument of GRACE: GPS augments gravity measurements, GPS World, 14, 16–28, 2003.

Houweling, S., Kaminski, T., Dentener, F., Lelieveld, J., and Heinmann, M.: Inverse modeling of methane sources and sinks using adjoint of a global transport model, J. Geophys. Res., 104, 26137–26160, doi:10.1029/1999JD900428, 1999.

Huffman, G. J., Adler, R. F., Bolvin, D. T., Gu, G., Nelkin, E. J., Bowman, K. P., Hong, Y., Stocker, E. F., and Wolff, D. B.: The TRMM Multisatellite Precipitation Analysis (TMPA): Quasiglobal, multiyear, combined-sensor precipitation estimates at fine scales, J. Hydrometeorol., 8, 3855, doi:10.1175/JHM560.1, 2007.

Kim, H., Yeh, P. J.-F., Oki, T., and Kanae, S.: Role of rivers in the seasonal variations of terrestrial water storage over global basins, Geophys. Res. Lett., 36, L17402, doi:10.1029/2009GL039006, 2009.

Koster, R. D., Suarez, M., Ducharne, A., Stieglitz, M., and Kumar, P.: A catchment-based approach to modeling land surface processes in a general circulation model. Part 1: Model structure, J. Geophys. Res., 105, 24809–24822, 2000.

Koster, R. D., Dirmeyer, P. A., Hahmann, A. N., Ijpelaar, R., Tyahla, L., Cox, P., and Suarez, M. J.: Comparing the degree of landatmosphere interaction in four atmospheric general circulation models, J. Hydrometeorol., 3, 363–375, 2002.

Knighton, E.: Fluvial forms and processes: A new perspective, Edward Arnold, London, 383 pp., 1998.

Lawrence, D. M. and Slater, A. G.: Incorporating organic soil into a global climate model, Clim. Dynam., 30, 145–160, 2007.

Laws, K. B., Janowiak, J. E., and Huffman, J. G.: Verification of rainfall estimates over Africa using RFE, NASA MPA-RT and CMORPH, AMS 18th Conference on Hydrology, Seattle, Washington, 2004.

Lee, H., Durand, M., Jung, H. C., Alsdorf, D., Shum, C. K., and Sheng, Y.: Characterization of surface water storage changes in Arctic lakes using simulated SWOT measurements, Int. J. Remote Sens., 31, 3931–3953, 2010.

Lehner, B. and Döll, P.: Developement and validation of a global database of lakes, 881 reservoirs and wetlands, J. Hydrol., 296, 1–22, 2004.

Leon, J. G., Calmant, S., Seyler, F., Bonnet, M.-P., Cauhopé, M., Frappart, F., Filizola, N., and Fraizy, P.: Rating curves and estimation of average water depth at the upper Negro River based on satellite altimeter data and modeled discharges, J. Hydrol., 328, 481–496, 2008.

Leopold, L. B., Wolman, M. G., and Miller, J. P.: Fluvial Processes in Geomorphology, W. H. Freeman, New York, 1964.

Lunetta, R. S., Knight, J. F., Ediriwickrema, J., Lyon, J. G., and Worthy, L. D.: Land-cover change detection using multitemporal MODIS NDVI data, Remote Sens. Environ., 105, 142–154, 2006.

Lyon, J. G., Yuan, D., Lunetta, R. S., and Elvidge, C. D.: A change detection experiment using vegetation indices, Photogramm. Eng. Rem. S., 64, 143–150, 1998.

Mahe, G., Bamba, A., Soumaguel, A., Orange, D., and Olivry, J.-C.: Water losses in the inner delta of the River Niger: water balance and flooded area, Hydrol. Process., 23, 3157–3160, doi:10.1002/hyp.7389, 2009.

Matthews, E.: Wetlands, in Atmospheric Methane: Its Role in the Global Environment, edited by: Khalil, M. A. K., Springer, New York, 202–233, 2000.

Meynadier, R., Bock, O., Guichard, F., Boone, A., Roucou, P., and Redelsperger, J.-L.: The West African Monsoon water cycle. Part I: a hybrid water budget dataset, J. Geophys. Res., 115, D19106, doi:10.1029/2010JD013917, 2010.

Miller, J. R., Russell, G. L., and Caliri, G.: Continental scale river flow in climate models, J. Climate, 7, 914–928, doi:10.1175/1520-0442(1994)007¡0914:CSRFIC¿2.0.CO;2, 1994.

Molod, A., Salmun, H., and Waugh, D.: The Impact on a GCM Climate of an Extended Mosaic Technique for the Land – Atmosphere Coupling, J. Climate, 17, 3877–3891, 2004.

Moody, J. A. and Troutman, B. M.: Characterization of the spatial variability of channel morphology, Earth Surf. Proc. Land., 27, 1251–1266, 2002.

Noilhan, J. and Planton, S.: A simple parameterization of land surface processes for meteorological models, Mon. Weather Rev., 117, 536–549, doi:10.1175/1520-0493(1989)117¡0536:ASPOLS¿2.0.CO;2, 1989.

Oki, T. and Sud, Y. C.: Design of total runoff integrating pathways (TRIP), Earth Interact., 2, 136, doi:10.1175/1087-3562(1998)002¡0001:DOTRIP¿2.3.CO;2, 1998.

Oki, T., Nishimura, T., and Dirmeyer, P.: Assessment of annual runoff from land surface models using Total Runoff Integrating Pathways (TRIP), J. Meteorol. Soc. Jpn., 77, 235–255, 1999.

Papa, F., Guntner, A., Frappart, F., Prigent, C., and Rossow, W. B.: Variations of surface water extent and water storage in large river basins: A comparison of different global data sources, Geophys. Res. Lett., 35, L11401, doi:10.1029/2008GL033857, 2008.

Papa, F., Durand, F., Rossow, W. B., Rahman, A., and Bala, S. K.: Satellite altimeter derived monthly discharge of the Ganga Brahmaputra River and its seasonal to interannual variations from 1993 to 2008, J. Geophys. Res., 115, C12013, doi:10.1029/2009JC006075, 2010a.

Papa, F., Prigent, C., Aires, F., Jimenez, C., Rossow, W. B., and Matthews, E.: Interannual variability of surface water extent at the global scale, 1993–2004 , J. Geophys. Res.-Atmos., 115, D12111, doi:10.1029/2009JD012674, 2010b.

Pierre, C., Bergametti, G., Marticorena, B., Mougin, E., Lebel, T., and Ali, A.: Pluriannual comparisons of satellite based rainfall products over the Sahelian belt for seasonal vegetation modelling, J. Geophys. Res., 116, D18201, doi:10.1029/2011JD016115, 2011.

Portmann F. T., Siebert, S., and Döll, P. : Global monthly irrigated and rainfed crop areas 926 around the year 2000: A new hight-resolution data set for agricultural and hydrological 927 modeling. Global Biogeochem. Cy., 24, GB1011, doi:10.1029/2008GB003435, 2010.

Prigent, C., Matthews, E., Aires, F., and Rossow, W. B.: Remote sensing of global wetland dynamics with multiple satellite data set, Geophys. Res. Lett., 28, 4631–4634, 2001.

Prigent, C., Papa, F., Aires, F., Rossow, W. B., and Matthews, E.: Global inundation dynamics inferred from multiple satellite observations, 1993–2000, J. Geophys. Res., 112, D12107, doi:10.1029/2006JD007847, 2007.

Redelsperger, J.-L., Thorncroft, C. D., Diedhiou, A., Lebel, T., Parker, D. J., and Polcher, J.: African Monsoon Multidisciplinary Analysis: An international research project and field campaign, B. Am. Meteorol. Soc., 87, 1739–1746, 2006.

Roddel, M., Velicogna, I., and Famiglietti, J. S.: Satellite-based estimates of groundwater depletion in India, Nature, 460, 999–1003, doi:10.1038/nature08238, 2009.

Rodriguez, E.: SWOT science requirements Document, JPL document, Initial release, 2009.

Rodriguez, E. and Moller, D.: Measuring surface water from space, Eos Trans. AGU, 85, Fall Meet. Suppl., Abstract H22C-08, 2004.

Sausen, R., Schubert, S., and Dumenil, L.: A model of river runoff for use in coupled atmosphere ocean models, J. Hydrol. Amsterdam, 155, 337–352, doi:10.1016/0022-1694(94)90177-5, 1994.

Sheffield, J., Goteti, G., and Wood, E. F.: Development of a 50-year high-resolution global data set of meteorological forcings for land surface modeling, J. Climate, 19, 3088–3111, 2006.

Swenson, S., Wahr, J., and Milly, P.: Estimated accuracies of regional water storage variations inferred from the Gravity Recovery and Climate Experiment (GRACE), Water Resour. Res., 39, 1223, doi:10.1029/2002WR001808, 2003.

Tapley, B. D., Bettadpur, S., Ries, J. C., Thompson,P. F., and Watkins, M. M.: GRACE measurements of mass variability in the Earth system, Science, 305, 503–505, 2004.

Taylor, C. M.: Feedbacks on precipitation from an African wetland, Geophys. Res. Lett., 37, L05406, doi:10.1029/2009GL041652, 2010.

Taylor, C. M., Gounou, A., Guichard, F., Harris, P. P., Ellis, R. J., Couvreux, F., and De Cauwe, M.: Frequency of Sahelian storm initiation enhanced over mesoscale soil-moisture patterns, Nat. Geosci., 4, 430–433, doi:10.1038/ngeo1173, 2011.

Verdin, K. L. and Greenlee, S. K.: Development of continental scale digital elevation models and extraction of hydrographic features, in: Proceedings, Third International Conference/Workshop on Integrating GIS and Environmental Modeling, Santa Fe, New Mexico, 21–26 January 1996, National Center for Geographic Information and Analysis, Santa Barbara, California, 1996.

Vergnes, J.-P., Decharme, B., Alkama, R., Martin, E., Habets, F., and Douville, H.: A Simple Groundwater Scheme for Hydrological and Climate Applications: Description and Offline Evaluation over France, J. Hydrometeorol., online first: doi:10.1175/JHM-D-11-0149.1, 2012.

Vermote, E., El Salleous, N., and Justice, C. O.: Atmospheric correction of MODIS data in the visible to near infrared: first results, Remote Sens. Environ., 83, 97–111, 2002.

Vorosmarty, C. J., Moore III, B., Grace, A. L., Gildea, M. P., Melillo, J. M., Peterson, B. J., Rastetter, E. B., and Steudler, P. A.: Continental scale models of water balance and fluvial transport: An application to South America, Global Biogeochem. Cy., 3, 241–265, doi:10.1029/GB003i003p00241, 1989.

Wahr, J., Swenson, S., Zlotnicki, V., and Velicogna, I.: Timevariable gravity from GRACE: First results, Geophys. Res. Lett., 31, L11501, doi:10.1029/2004GL019779, 2004.

Wigneron, J. P., Calvet, J. C., Pellarin, T., Van de Griend, A., Berger, M., and Ferrazzoli, P.: Retrieving near-surface soil moisture from microwave radiometric observations: current status and future plans, Remote Sens. Environ., 85, 489–506, 2003.

Yamazaki, D., Oki, T., and Kanae, S.: Deriving a global river network map and its sub-grid topographic characteristics from a fine-resolution flow direction map, Hydrol. Earth Syst. Sci., 13, 2241–2251, doi:10.5194/hess-13-2241-2009, 2009.

Yamazaki, D., Kanae, S., Kim, H., and Oki, T.: A physically-based description of floodplain inundation dynamics in a global river routing model. Water Resour. Res. 47, W04501, doi:10.1029/2010WR009726, 2011.

Zagona, E. A., Fulp, T. J., Shane, R., Magee, T., and Goranflo, H. M.: RiverWare: A generalized tool for complex reservoir system modeling, doi:10.1111/j.1752-1688.2001.tb05522.x, 2001.